Geological Magazine

www.cambridge.org/geo

Hydrothermal injection breccia with organic carbon and nitrogen in the fossil hydrothermal system of Harghita Bãi, East Carpathians, Romania: an example of magmatic and non-magmatic element mobility in the upper continental crust

Iuliu Bobos

ICTerra-Porto, Faculty of Sciences, University of Porto, Rua do Campo Alegre 689, 4168-007 Porto, Portugal

Original Article

Cite this article: Bobos I (2023) Hydrothermal injection breccia with organic carbon and nitrogen in the fossil hydrothermal system of Harghita Bãi, East Carpathians, Romania: an example of magmatic and non-magmatic element mobility in the upper continental crust. *Geological Magazine* **160**: 274–291. https://doi.org/10.1017/S0016756822000851

Received: 28 November 2021
Revised: 18 July 2022
Accepted: 19 July 2022
First published online: 24 October 2022

Keywords:
calc-alkaline Neogene volcanism; breccia textures; organic carbon and nitrogen; K- and NH_4-illite clays; HFSE and REE geochemistry; stable isotopes; Harghita Bãi; Romania

Author for correspondence:
Iuliu Bobos, Email: ibobos@fc.up.pt

Abstract

Organic carbon and nitrogen fixed in illite (I) clays were identified in a hydrothermal breccia structure from the Harghita Bãi area of the Neogene volcanism of the East Carpathians. The potassium-illite (K-I) alteration related to an early magmatic-hydrothermal event (9.5 ± 0.5 Ma) was later replaced by ammonium-illite (NH_4-I) (6.2 ± 0.6 Ma) owing to circulation of an organic-rich fluid. Several textural evolutions of breccia structures were recognized, such as 'shingle', 'jigsaw', 'crackle' and hydraulic *in situ* fractures. The high-field-strength element behaviours of the K-I and NH_4-I argillic altered andesite are close to chondritic ratios, indicating no contribution of hydrothermal fluid, especially on NH_4-I andesite alteration and the CHArge-and-RAdius-Controlled (CHARAC) behaviour within silicate melts. The rare earth element normalized patterns show two distinct trends, one with a Eu* anomaly (K-I) and the other with a Nd* anomaly (NH_4-I), indicating a boundary exchange with the organic-rich fluid. The strongly depleted $\delta^{13}C$ (V-PDB) measured for the NH_4-I clays reflects values (−24.39 to −26.67 ‰) close to CH_4 thermogenic oxidation, whereas the $\delta^{15}N$ (‰) from 4.8 to 14.8 (± 0.6) confirmed that the N_2 originated from post-mature sedimentary organic matter. The last volcanism (6.3 to 3.9 ± 0.6 Ma) and simultaneous volcano-induced tectonics in the proximity of the eastern Transylvanian basin basement increased the heat flow, generating lateral salt extrusion, diapirism and increased pressure in the gas reservoir. New pathways were opened that provided new circulation routes for basinal fluids to new and old permeable zones and expelled seeps from the biogenic petroleum system.

1. Introduction

Large areas containing occurrences of volcanic, endogenic and hydrothermal breccia structures are associated with terranes, provinces and belts related to geological settings (i.e. subduction, collisional plates, etc.). These are produced either by volcanic chains or intrusive granitoid bodies.

Volcanic breccias form large parts of composite volcanoes and are commonly viewed as containing pyroclastic fragments emplaced by pyroclastic processes (Wright *et al.* 1980). Most volcanic breccias are interpreted as debris-flow or sheetwash deposits with a dominant pyroclastic matrix and containing mixed material of autoclastic or alloclastic and pyroclastic origin. Usually, autoclastic breccias include the products of fragmentation of semi-solid lava by its own movement (*friction-breccia*, *flow-breccia*) and the products of the explosion of gases within lavas, whereas alloclastic breccias result from the fragmentation of pre-existing rocks by volcanic-related processes beneath the surface (Wright & Bowes, 1963).

Endogenic and hydrothermal breccia structures were recorded in the Cordilleran–Andean belt, Circum-Pacific belt, European Variscan orogenic belt (i.e. Cornubian Hercynic granitoids, French Massif Central, Iberian Massif, etc.), and Neogene volcanism of the Carpathian arc, among others, where most of the breccia structures are mineralized. Associations of breccias with ores in a variety of mineralization types and settings have been reported in relation to porphyry copper systems (Sinclair, 2007; Sillitoe, 2010 among others), W-mineralization (Harlaux *et al.* 2019) and Au–Ag precious metals (Sillitoe, 1985; Goldfarb *et al.* 2005; Zhang *et al.* 2019).

A complex study dedicated to breccia formation and its evolution related to a variety of base and precious metals and lithophile elements in a volcano-plutonic arc was carried out by Sillitoe (1985), from which several possible mechanisms for subsurface brecciation were drawn. The most abundant and widespread breccias are associated within porphyry copper systems, gold,

molybdenum, tin or tungsten deposits. The Lowell & Guilbert (1970) and dioritic models (Hollister, 1978), related to porphyry copper systems, have associated breccia pipe structures with a halo alteration–mineralization described in several deposits from the United States (Bingham, Utah; Bagdad, Arizona), Chile (El Teniente) and Peru (Toquepala), among others. Also, tourmaline breccia structures associated with Sn–W metallogenesis (Goode & Taylor, 1980; Allman-Ward *et al.* 1982; Harlaux *et al.* 2019) were described across the European Variscan belt within the Cornubian Hercynic granitoids (Cornwall, England) and French Massif Central (Le Puy, France), exhibiting certain similarities with those from the Bolivian tin belt (Sillitoe *et al.* 1975).

Deep sedimentary basins affected by the circulation of magmatic fluids or by the intrusion of igneous rocks may result in the migration of a combination of fluids, hot water and gases, with hybrid geological systems, hosting both volcano-hydrothermal and sedimentary components, being first recognized by Svensen *et al.* (2003). Piercement structures (i.e. hydrothermal vent complexes) associated with the escape of over-pressured fluids may represent important secondary migration pathways for basinal fluids, including petroleum (Svensen *et al.* 2003, 2006, 2007, 2008; Jamtveit *et al.* 2004). There are many cases around the world where magmatic intrusions and volcanic plumbing systems occur within sedimentary basins resulting in hybrid systems with both CO_2-rich geothermal fluids and CH_4-rich biogenic gas (microbial or thermogenic) sourced from organic-rich sediments (Procesi *et al.* 2019). Thus, unexplained exotic hydrocarbon reservoirs have been found in volcanic rocks distributed along the Pacific Rim, Africa and Central Asia (Schutter, 2003*b*) in the last 20 years. According to Schutter (2003*a*), more than 100 volcanic gas fields with proven reserves have been found in various countries such as the United States (Gries *et al.* 1997), Venezuela (Rohrman, 2007), Argentina (Sruoga & Rubinstein, 2007), Japan (Sakata *et al.* 1997; Tomarua *et al.* 2009) and China, where favourable targets for natural gas exploration were delimited in volcanic rocks from China (Feng, 2008; Wang *et al.* 2008).

An unmineralized hydrothermal breccia structure with organic carbon and nitrogen fixed in clay minerals (argillic alteration) was identified in the fossil hydrothermal system of Harghita Băi from the Neogene volcanism of the East Carpathians (Romania) (Bobos, 2012). This breccia structure type is unusual owing to the presence of organic-N fixed in illitic clays within the argillic alteration developed along the breccia structure. This study combined field and descriptive observations carried out on the breccia architecture, complemented by mineralogical and geochemical data (high-field-strength elements (HFSEs), rare earth elements (REEs) and ^{13}C, ^{15}N, ^{18}O isotopes) for whole argillic rocks, ammonium-illite (NH_4-I) clay fractions and quartz crystals collected from the breccia structure, in order to identify the source of the palaeofluid circulation. In particular, the ^{13}C and ^{15}N isotopes measured on NH_4-I clays represent tracers of fluid flow circulation in the fossil hydrothermal system of Harghita Băi, which contributed to a late NH_4-I alteration, with higher amounts of NH_4 fixed in the illite lattice structure at temperatures up to 300 °C.

2. Geological background

2.a. Regional geology

The Neogene volcanic activity from the East Carpathians represents a subsequent stage of magmatism associated with the Carpathian orogen, with the calc-alkaline volcanism (Miocene and Pliocene) considered to be related to subduction of the East European Plate and Inner-Carpathian area beneath the Alpaca and Tisza–Dacia microplate (Fig. 1a) (Seghedi *et al.* 1998). The Călimani–Gurghiu–Harghita (CGH) volcanic chain, known for its diminishing volume and age southwards from 10 to 3.9 Ma, consists of calc-alkaline products displayed along the easternmost margin of the rigid Tisza–Dacia block (Szakács & Seghedi, 1995). This marks the end of the post-collisional subduction-related magmatism along the front of the European convergent plate margin (Seghedi *et al.* 1998). A post-collisional setting was suggested, where a large volume of calc-alkaline magma was formed along the trans-tensional faults (e.g. at the margins of the Transylvanian basin) at destructive boundaries (Mason *et al.* 1998; Seghedi & Downes, 2011). The locations of the eruption centres in the CGH chain are concentrated at intersections with the crustal fault system propagated from N to S along the arc at the eastern boundary of Tisza–Dacia block, suggesting a NNW–SSE-striking sinistral trans-tensional faulting (Fielitz & Seghedi, 2005).

The interaction between the volcanic edifices and pre-volcanic basement of the eastern Transylvanian basin was deduced from the topographic and tectonic features and inferred from geological and geophysical data (Szakács & Krézsek, 2006; Krézsek & Bally, 2006). The Transylvanian basin, consisting of the Dacia block and NE Tisza block, displayed a minor Miocene upper crustal extension, which was replaced during Late Miocene time by small-scale contraction features and shallow salt diapirs (Krézsek & Bally, 2006; Mațenco *et al.* 2010). The pre-volcanic basement of the western part of the CGH chain boundary with the Tisza–Dacia block consists of a thick sedimentary pile, including ductile rocks such as clay and salt that are prone to plastic deformation (Krézsek & Bally, 2006).

2.b. The Călimani–Gurghiu–Harghita volcanic arc

The CGH volcanic chain (Fig. 1b) is the youngest unit of the Carpathian arc, being formed within a regional context of igneous activity migration in time and space from northwest to southeast (Central Slovakia to Eastern Carpathians), with a volcanic evolutionary trend from acid to basic being assigned. The Călimani Mountains (north) are the larger and older stratovolcano, whereas the Harghita Mountains (south) are the younger volcanic centre. The volcanic activity developed from the north to the south of the volcanic chain along several stratovolcano centres from Late Miocene (12 Ma) to Quaternary (0.2 Ma) times (Pecskay *et al.* 1995), with 18 major volcanic centres being recognized along the CGH volcanic chain.

Magmatic activity was developed after the thrust emplacement of the flysch and molasse zones from the East Carpathians. The thickness of the flysch and molasse sediments is ~6–7 km (Roure *et al.* 1993), and they crop out to the east of the CGH volcanic chain, suggesting that only a small proportion of the sediments was subducted overlying the downing plate (Seghedi *et al.* 1998). Also, the continental metamorphic basement (Precambrian metamorphic rocks and Mesozoic sedimentary cover) cropping out east of the volcanic arc was tectonically active during the Variscan and Alpine orogenesis (Pana & Erdmer, 1994).

The parental magma assimilated metamorphic rocks in the northern Harghita and Gurghiu mountains, whereas flysch sediments contaminated the parental magmas in the southern Harghita and Călimani (Mason *et al.* 1996). Therefore, andesite magmas erupted through the crustal basement, assimilating a variety of rocks during their ascent to the surface.

https://doi.org/10.1017/S0016756822000851 Published online by Cambridge University Press

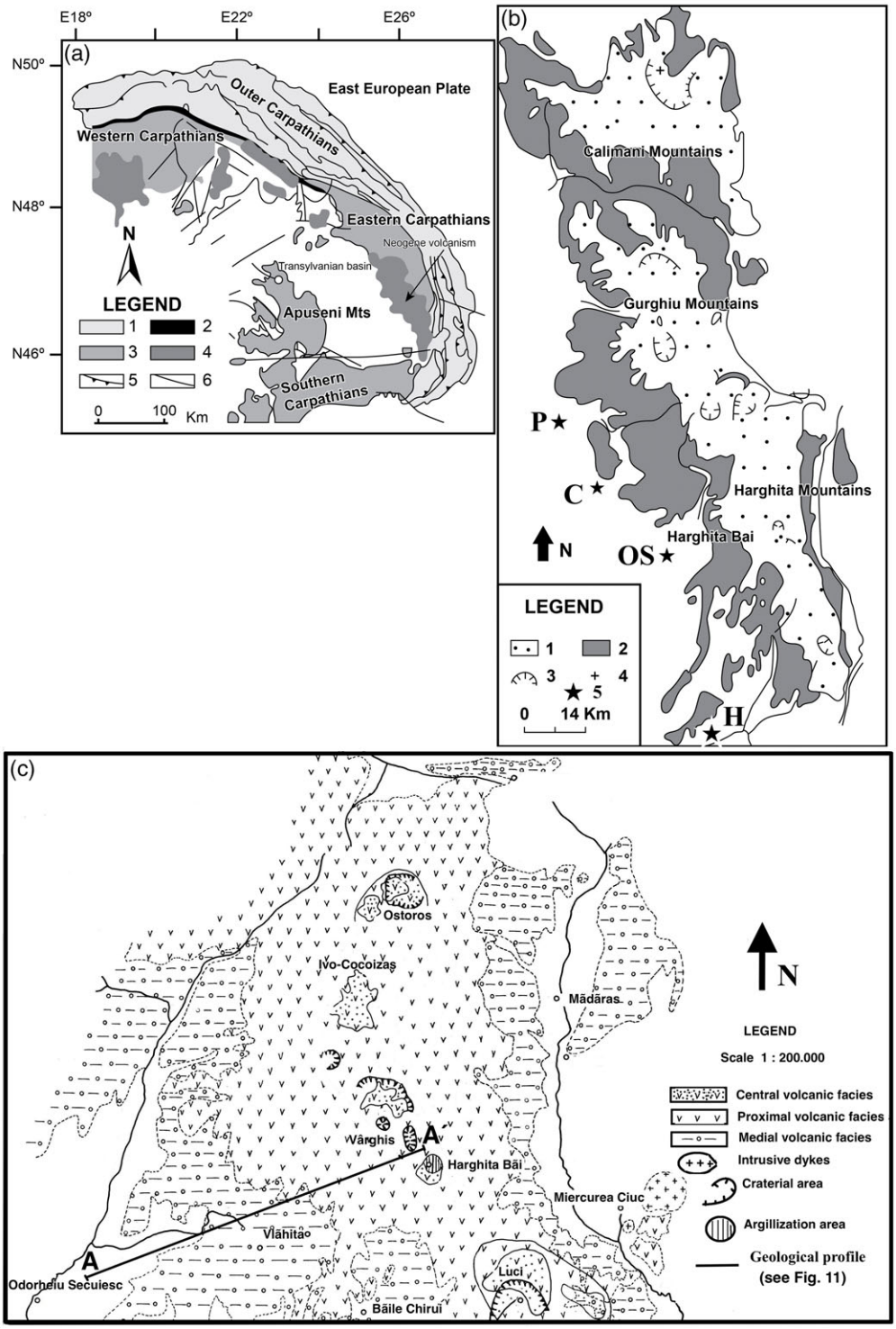

Fig. 1. (a) Geotectonic sketch of the Carpatho-Pannonian area (Royden, 1988; Seghedi *et al*. 1998, 2004) showing major tectonic units and boundaries, and the main areas of the Neogene calc-alkaline volcanic rocks. Legend: 1 – Outer Carpathians (Moldavide); Neogene–Quaternary sediments and flysch nappes; 2 – Pieniny klippe belt; 3 – pre-Neogene rocks of the inner Alpine – Carpathian Mountains; 4 – Neogene calc-alkaline volcanic areas; 5 – major thrusts; 6 – strike-slip faults. Reproduced from Bobos & Eberl (2013) with permission of Springer Nature. (b) Geological sketch of the Călimani–Gurghiu–Harghita volcanic arc, Eastern Carpathians (Szakacs & Seghedi, 1995). Legend: 1 – upper structural compartment (central or 'core' and proximal or 'flank' facies model). The central facies is constituted by eroded central volcanic depressions, the crater and/or caldera remnants and eruptive vents, whereas the proximal facies corresponds to lava flows and subordinate pyroclastic interbeds, which accompany the modified outer slopes of the volcanic edifices (Szakacs & Seghedi, 1995); 2 – lower structural compartment (peripheral distal or volcaniclastic facies, which surround the base of volcanoes); 3 – crater area; 4 – centres of eruptions; 5 – seeps and volcanic muds. The Harghita Băi hydrothermal area is indicated by an arrow. Also, the seeps and volcanic muds (P – Praid; C – Corund; OS – Odorheiu Secuiesc; H – Homorod) located on the eastern margin of the Transylvanian basin. Reproduced from Bobos & Eberl (2013) with permission of Springer Nature. (c) Geological map of the northern Harghita Mountains and location of the Vârghis–Harghita Băi stratovolcano.

https://doi.org/10.1017/S0016756822000851 Published online by Cambridge University Press

2.c. The volcanic structure of Vârghis–Harghita Bãi

The CGH volcanic chain is viewed as an ideal volcanic structure, consisting of a central volcanic zone having an infrastructure of subvolcanic bodies, with an intermediate zone corresponding to a volcanic cone and a peripheral volcaniclastic zone (Szakacs & Seghedi, 1995). The volcanic structure of Vârghis–Harghita Bãi (VHB) is situated in the northern sector of the Harghita Mountains (Fig. 1c), where the volcanic edifice had a multi-stage evolution including a stratovolcanic and intrusive stage. The volcaniclastic compartment represents a distal peri-volcanic facies as volcanic fans or aprons, whereas the stratovolcanic compartment represents a central facies with complex craters and calderas modified by erosion (Szakacs & Seghedi, 1995).

The Harghita Bãi eruptive structure situated in a craterial area joins the stratovolcanic compartment consisting of a deep microdiorite to andesite formation preceding a great variety of andesitic rocks developed to the surface. The post-failure activity developed along the CGH volcanic chain generated several lava centres in the region, including several late-stage andesitic lava extrusions (i.e. Harghita Ciceu, Borhegy, etc.), which partly obtrude the older Harghita Bãi intracraterial area (Szakacs & Seghedi, 1995). The absolute ages of the andesitic rocks corresponding to the intermediate zone of the VHB stratovolcanic structure range from 6.3 to 3.9 Ma (Late Pliocene; Peltz *et al.* 1987; Pecskay *et al.* 1995).

2.d. The fossil hydrothermal system of Harghita Bãi

The 'fossil' hydrothermal system of Harghita Bãi resulted from complex hydrothermal activity, well-established in a given geotectonic setting as being the result of a volcano-plutonic hydrothermal system evolution. The magmatic-hydrothermal fluids related to the evolution of the subvolcanic body (i.e. microdiorite) generated this hydrothermal system. A wide variety of calc-alkaline andesites (e.g. basaltic andesite, amphibole ± pyroxene ± biotite andesite) occur above the subvolcanic body. The alteration halo (biotite → amphibole → phyllic → argillic) centred on the intrusive dioritic body and subvolcanic body (Fig. 2) was probably associated with the evolution of a porphyry copper system (Stanciu, 1984).

The hydrothermal area of Harghita Bãi was investigated from the surface to a depth of −110 m, where a hydrothermal injection breccia structure containing NH_4-illite–smectite (I–S) mixed-layers (40–5 %S) was identified for the first time (Bobos & Ghergari, 1999; Bobos, 2012). The NH_4-I–S clays occur in the barren part of the breccia structure, where a conversion series of smectite to NH_4-I–S ordered mixed-layered (40–5 %S) and K-I/NH_4,K-I mixed phases (outside of the breccia structure at −110 m in mine drifts) were identified (Bobos, 2012, 2019; Bobos & Eberl, 2013). K–Ar dating of the K-I/NH_4,K-I mixed phases yielded an age of 9.5 ± 0.5 Ma, whereas the NH_4-I collected from the bottom of the breccia structure (−110 m) yielded a younger age of 6.2 ± 0.6 Ma (Clauer *et al.* 2010).

A large number of CO_2-rich cold springs, CO_2-rich gas vents ('*mofettes*'), dry fumaroles and CO_2 gas discharged to the surface are well known within the volcanic edifices of the Harghita Mountains and across the CGH volcanic chain as well (Rãdulescu *et al.* 1981; Crãciun & Bandrabur, 1993). The large circulation of fluids (+ gases) in the Harghita volcanic area was triggered by the presence of mantle-derived magmas, where the total ^3He came from the mantle or from degassing of magmas stored in the crust, and the CO_2 from either volcanic degassing or metamorphism of recently subducted limestones (Vaselli *et al.* 2002).

3. Materials, sample preparation and methods

3.a. Materials

The NH_4-I-bearing argillized andesite rocks were collected from the mine drifts and shafts located at depths of −30, −50, −80 and −110 m, where a broad argillization zone occurs exceeding more than 100 m in depth (studied area). Whole NH_4-I argillized rocks were submitted for mineralogical and chemical analysis. Clay fractions of <2 μm were extracted from whole rocks for mineralogical and stable isotope geochemistry. A complete series of NH_4-I–S mixed-layers (here after NH_4-I clays) were identified at different levels within the breccia structure (Bobos, 2012; Bobos & Eberl, 2013), including a mechanical mixture of potassium-illite (K-I) and (NH_4,K)-I mixed-layers (hereafter K-I/NH_4,K-I clays) identified at −110 m outside of the breccia structure (Bobos, 2019).

3.b. Clay sample preparation

The chemical treatments of the clay samples followed M. L. Jackson's (1975) method. In brief, the samples were treated with Na-acetate (NaOAc) to remove carbonate (pH = 5.5; T = 100 °C). Fe oxyhydroxides were reduced using Na-dithionite and Na-citrate (pH = 7; T ~80 °C). The salt excess was removed from the <2.0 μm clay fractions by washing in distilled-deionized water followed by dialysis.

The samples were washed several times after saturation with each inorganic complex in a 1:1 deionized water – ethanol mixture until chloride-free, based on the $AgNO_3$ test, which confirmed the complete removal of Cl^- ions. The oriented clay mounts were ethylene glycol solvated for 8 hours at 60 °C, prior to X-ray diffraction (XRD), and compared to air-dried patterns. The <2.0 μm size fraction was separated by successive dispersion and sedimentation cycles in distilled water according to Stoke's Law; the clay fractions were concentrated by centrifugation and re-dispersed with an ultrasonic probe.

3.c. Analytical techniques

3.c.1. X-ray diffraction

XRD patterns of oriented specimens were obtained using a Rigaku Geigerflex D/max.–C series automated diffraction system equipped with a graphite monochromator and using CuKα radiation. Samples were analysed in the range 2–50° 2θ, using a 1° divergence slit, a step size of 0.05° 2θ and a counting time of 5 s/step.

3.c.2. Infrared spectroscopy

Pellet discs of 15 mm were prepared by mixing 1 mg of sample (<2 μm fraction) with 200 mg KBr and then pressing at 14 kg cm^{-2}. Prior to analysis, the pellets were heated overnight at 150 °C to remove any adsorbed water. The samples were studied in the absorption mode using a Bruker Tensor 27 spectrometer equipped with a deuterated triglycine sulfate (DTGS) single detector plate. The infrared (IR) spectra were recorded in the 4000–400 cm^{-1} frequency region. The measurements of the integrated intensity of the molecular vibration bands were made using the OPUS 4.2® software supplied by Bruker.

3.c.3. Scanning electron microscopy

Small pieces (5–8 mm in diameter) of argillized rocks were mounted on a carbon holder and sputter-coated with a thin carbon film for conductivity. The scanning electron microscopy (SEM) study was performed with a Hitachi S-4100 electron microscope operated at an accelerating voltage of 25 kV and 5 nA beam

https://doi.org/10.1017/S0016756822000851 Published online by Cambridge University Press

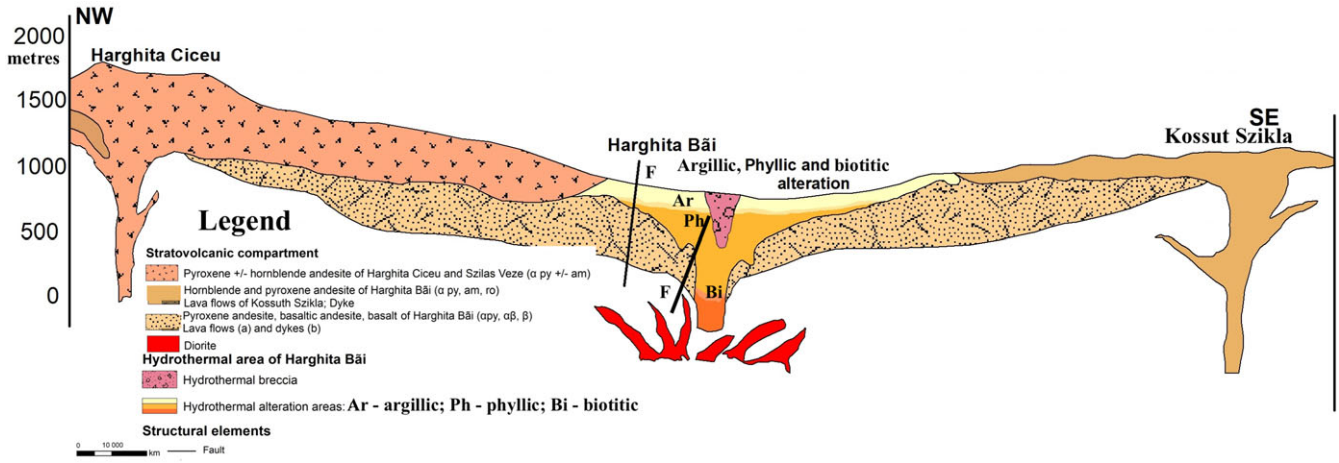

Fig. 2. (Colour online) Schematic cross-section through the fossil hydrothermal system of Harghita Băi illustrating salient features of the hydrothermal alteration zones and the hydrothermal breccia location.

current, equipped with an X-ray energy-dispersive spectral (EDS) spectrometer (Oxford Instruments INCA energy). A 200 nm spot size and 100 s of live time were used.

3.c.4. Inductively coupled plasma mass spectrometry

Major-, trace- and REE chemistry were measured on whole altered and fresh rocks by inductively coupled plasma mass spectrometry (ICP-MS) at Actlabs (Ancaster, Ontario, Canada). Prior to analysis by ICP-MS, the whole rocks underwent a lithium metaborate/tetraborate fusion, which rapidly dissolved in nitric acid. Actlabs uses a fusion process that guarantees precise total metal analyses, particularly for REEs and trace elements in resistant phases (Hoffman, 1992; https://www.actlabs.com). Calibration was carried out using the international standards used by Actlabs (GXR-1, NIST 694, DNC-1, GBW 07113, GXR-4, SDC-1, GXR-6, LKSD-3, LKSD-4, BaSO4, W-2a, SY-4, CTA-AC1, BIR-1a, NCS DC70014, NCS DC70009, OREAS 100a, OREAS 101a, OREAS 98, JR-1, DNC-1a, OREAS 13B). The analytical precision calculated between the measured and certified values of the standards is ±3 % for all elements. The reproducibility of the results was confirmed by the duplicate samples sent with the package. The measurement precision for major elements is within the 1–2 % interval, whereas it is better than 5–10 % for trace elements. For REEs, the measurement precision was 5 % or better. Accuracy was verified with laboratory standards run simultaneously. The REE data were plotted against the Upper Continental Crust (UCC) normalization reference (Rudnick & Gao, 2003) in order to visualize the fractionation processes of either light REEs (LREEs) relative to medium REEs (MREEs) or heavy REEs (HREEs).

3.c.5. Organic elemental analyser

Carbon–nitrogen–hydrogen–sulfur (C–N–H–S) were measured with a Thermo Finnigan, Flash 2000 in the Department of Chemistry of the University of Aveiro (Portugal). Standard and replicated samples were used for quality control with a relative analytical error of <2 %. About 30 mg of ground sample were weighed and filled into tin cups for the C–N–H–S measurements.

3.c.6. Conventional isotope ratio mass spectrometry

The carbon content and $\delta^{13}C$ isotopic compositions were measured with an elemental analyser coupled to a DELTAplusXL (ThermoFischer) isotopic ratio mass spectrometer in the Keck Laboratories of Arizona State University (Tempe, AZ, USA). Carbon contents were measured on bulk argillic andesite rocks and clay fractions, whereas the $\delta^{13}C$ isotope analysis was carried out only on the <2 μm NH_4-I samples extracted from the bulk altered argillized andesite. The carbon isotopic compositions were expressed in the standard δ-notation in parts per mil (‰), as the relative difference between isotopic ratios in the sample and in conventional standards (Vienna Pee Dee Belemnite; V-PDB) for carbon ($\delta^{13}C = 0.0$ ‰; Craig, 1953). The $\delta^{13}C/^{12}C$ isotopic ratio in the clay fractions was analysed after dissolving samples in H_3PO_4, and the results are presented as per mil (‰) deviations with respect to V-PDB. The $\delta^{13}C$ values were calculated using the following equation:

$$\delta^{13}C\ (‰) = (((^{13}C/^{12}C)\text{sample}/(^{13}C/^{12}C)_{std}) - 1)*1000$$

The international graphite standard USGS 24 ($\delta^{13}C = -16.0 \pm 0.1$ ‰) was used for ^{13}C measurements. The reproducibility of isotopic compositions based on replicate measurements was ± 0.1 ‰ for $\delta^{13}C$ values, and the precision of analysis was ± 0.2–0.3 ‰ for $\delta^{13}C$.

3.c.7. Oxygen isotopes

Oxygen isotope analysis was carried out on quartz crystals collected from the breccia structure at −110 m and −80 m. Oxygen was extracted by reaction with BrF_5 at 550 °C in Ni reaction vessels (Clayton & Mayeda, 1963), converted to CO_2 and analysed in a double-collecting mass spectrometer. The results are given in the usual δ-notation in per mil relative to the SMOW standard as averages of duplicate determinations, with a precision of +0.2 ‰. The $\delta^{18}O$ value of the NBS-28 quartz standard was +9.6 ‰ during the course of the study.

4. Results

4.a. Geometry, shape and texture of breccia

Magmatic-hydrothermal breccia structures are described in the literature in terms of morphology, composition or ore-related mineralization event (Sillitoe, 1985; Laznicka, 1988; Reimold, 1998; Taylor & Pollard, 1993; Corbett & Leach, 1998; Davies *et al.* 2000 among others). The breccia structure from the Harghita

https://doi.org/10.1017/S0016756822000851 Published online by Cambridge University Press

Băi area is confined to a single space with a close genetic connection to a porphyry intrusive dyke and a crustal fracture (NE–SW), devoid of ores and with organic C and N elements fixed in illite argillic alteration. The exotic elements found in the hydrothermal alteration envelope increase the scientific interest.

Several mine drifts at –30 m, –50 m, –80 m and –110 m including shaft mining works were prospected underground in the former '*kaolin*' mine of Harghita Băi for detailed information concerning the geometry, shape and texture of the breccia. Extending breccia was verified laterally and vertically where a movement of the andesitic flow was observed from the bottom to upper part of the breccia structure.

The horizontal extension of the breccia structure was estimated at ~50 to 70 m and vertically ~150 m. The contact between the breccia and wall rock is net-like or marked by fractures observed in several places underground. Tuffaceous matrix or exotic rocks from a possible pre-volcanic fundament were not identified within the breccia matrices.

Apparently, gas explosions played a main role in the architecture of the breccia formation. The explosion character of the breccia could be related to reduced pressure above the magma column (Sillitoe & Sawkins, 1971), where the finest material deposited after the gas explosion (Perry, 1961) cemented the brecciated andesitic blocks or fragments. Movement of andesite blocks or fragments in rising gas show either irregular or rounded clasts at the top.

The top and bottom terminations of the breccia structure were identified underground at −30 m and −110 m. Andesitic blocks and fragments moved and collapsed after the gas explosion occurred at the top of the breccia structure. Angular to subrounded rock fragments ranging in size occur underground from 30− to −50 m. Rounded, spheroidal, elliptical or subangular clasts were observed (Fig. 3a), where fragments of andesite rocks of various sizes (15 to 50 cm) were argillized and caught in a flour groundmass. The rotation of clasts and the transition of the shapes of small andesite fragments (2–3 cm) from irregular polygons to elliptical (Fig. 3a) that are caught in a milled matrix occur only at the top of the breccia. Characteristically, both rounded clasts and elliptical fragments are aligned, keeping the same flow direction as significant hydrothermal fluid feeders.

A variety of similarly shaped clasts, in a chaotic texture and high amount of flour-milled rock groundmass, were also observed at the top of the breccia (Fig. 3b). The contact was controlled by a fracture or an external brittle fracture to the west of the breccia structure, where a sheared andesite material, strongly milled, could be observed. Parts of the breccia structure show multiple events of brecciation, cementation and re-brecciation (near a tectonic fault).

A '*cramble*' breccia occurs in several places caught in a flour-milled rock mass, where irregular andesitic blocks (~50 × 20 cm) with rounded edges or '*shingle*' blocks with a parallelepiped shape (Fig. 3c) were found at –80 or –90 m underground. The argillized andesite rocks are progressively displaced and tumbled into the small (20 to 40 cm) or larger disordered fragments of andesite to the outer limits at –80 m. Also, andesite blocks of 60 × 110 cm joined to small andesite blocks with a parallelepiped shape were identified (Fig. 3c). Part of the breccia structure with a '*shingle*' texture was formed by collapsed material after the gas explosion. This part of the breccia structure could be associated with a '*shingle breccia*' texture as a result of regular breakage and detachment of zones of sheeting like those around pipe walls and large fragments (Sillitoe, 1985).

A jigsaw or mosaic texture is observed in Figure 3d, where big and small clasts of andesite were fragmented or disrupted. Rotational 'blocks' are defined as breccias in which the blocks were disrupted by rotation of breccia clasts as a result of the introduction of additional matrix (Corbett & Leach, 1998). Small clasts observed (Fig. 3d) were weakly or strongly milled during rotation, where the fluidized matrix formed the cement between big or small angular argillized clasts.

A '*crackle*' breccia texture characterized by andesite fragments fitted back into their apparently initial position was observed at –80 m. In this region, the open-space-fillings are cemented by flour-rock, and an incipient argillic alteration was observed on the edges of andesite blocks (Fig. 3e).

A transitional stage to the main intrusive body (dyke) was observed towards the bottom at −110 m (Fig. 3f). Tension and shearing fissure system types were identified in the brecciated NH_4-I altered andesite dyke (Fig. 3f). The hydraulic fracturing of the andesite dyke occurred owing to a high-pressure gas explosion event (~100 MPa, after Guedes *et al.* 2000), generating '*crackle*' blocks. Cement and hydrothermal quartz crystals from the open-filling space of the breccia were collected from this location for mineralogy and geochemistry (see Table 1). The fractured andesitic spaces were filled by quartz, pyrite and tourmaline crystallized after a high-pressure gas explosion.

4.b. Alteration stages

During the protracted period related to a high-pressure gas explosion event, the fractured blocks and fragments of andesite rocks supported argillization across the breccia structure from −110 m to −30 m. The K-I alteration (at −110 m), older than the NH_4-I alteration, and a propylitic alteration (smectite) at −80 m occurs outside of the breccia structure. The NH_4-I with 5 % smectite (%S) content occurs at −110 m (Fig. 3f), interpreted as being the central zone of the breccia structure. NH_4-I–S ordered mixed-layers (the %S content ranging from 10 to 40 %) were identified at the top of the breccia structure at −80 m, −55 m and −30 m.

K–Ar data of K-I alteration yielded an age of 9.5 ± 0.5 Ma, whereas NH_4-I alteration yielded an age of 6 to 2 (± 0.5) Ma (Clauer *et al.* 2010). The spatial relationship between the NH_4-I alteration zone found within the breccia structure and the K-I and propylitic alteration stages is shown in Figure 4.

In general, the zonation of hydrothermal alteration often occurs from an illite zone (phyllic) at the centre, to a smectite zone (propylitic) at the margin, where such central zonation represents the effects of hydrothermal fluid circulation at a higher temperature where metals may have been deposited (Inoue *et al.* 1992).

4.c. Mineralogy

Bulk NH_4-I altered andesite rock shows a monotonous mineralogy composed of quartz, NH_4-I, Ca–Na feldspar (andesine), pyroxene, amphibole and small amounts of pyrite. The open-space filled by flour groundmass is predominantly composed of quartz (>75 %) and small amounts of pyrite (± marcasite), tourmaline, amphibole and pyroxene.

The mineralogy of the breccia structure is composed of NH_4-I–S clays where the evolution of NH_4-I crystal growth was simulated using the crystal growth theory of Eberl *et al.* (1998). The <2 μm clay fractions extracted from altered andesite rocks collected from −110 m (sample HB-18) contain NH_4-I and small amounts of quartz (<10 %). Changes in the mean crystallite thickness (T_{mean}) of NH_4-I–S (30 to 5 %S) from 2.8 nm to 7.1 nm for the <2 μm fractions were measured from –55 to −94 m by Bobos & Eberl (2013) (Fig. 4). NH_4-I found at *c.* −94 m (Fig. 3f) displays

https://doi.org/10.1017/S0016756822000851 Published online by Cambridge University Press

Table 1. Oxide chemical elements composition of NH_4-I and K-I/NH_4,K-I argillic alteration of andesite rocks

Rock samples	Mineralogical assemblages	SiO_2	TiO_2	Al_2O_3	Fe_2O_3	MgO	CaO	K_2O	Na_2O	H_2O	Total
327	NH_4-I/S, Kln, Q	64.78	0.84	18.81	3.20	3.15	1.34	1.04	0.10	6.74	100.00
320	NH_4-I/S, Q	65.63	0.69	18.30	3.33	3.87	0.77	0.66	0.06	6.69	100.00
321	NH_4-I/S, Q	65.08	0.70	20.97	1.97	2.83	0.46	0.54	0.10	7.35	100.00
324	NH_4-I/S, Q	64.82	0.79	19.38	2.79	2.47	0.51	1.34	0.48	7.42	100.00
314	NH_4-I/S, Q	64.38	0.91	20.46	2.38	1.94	0.64	1.62	0.55	7.12	100.00
352	NH_4-I/S, Q	63.34	0.72	21.33	1.72	2.11	0.79	2.14	0.36	7.49	100.00
211	NH_4-I/S, Q	64.65	1.06	20.85	1.57	2.17	0.48	1.57	0.14	7.51	100.00
340	NH_4-I, Q	62.34	0.91	22.74	1.89	2.56	0.32	1.68	0.21	7.35	100.00
346	NH_4-I, Q	61.79	0.84	22.93	1.75	1.54	0.47	1.47	1.64	7.57	100.00
150	K-I/NH_4.K-I, Q, Pirite	60.08	0.64	19.73	3.77	1.52	0.94	4.20	1.60	7.52	100.00
108a	Breccia cement	76.25	0.70	9.70	5.60	0.80	0.49	1.10	0.62	4.74	100.00

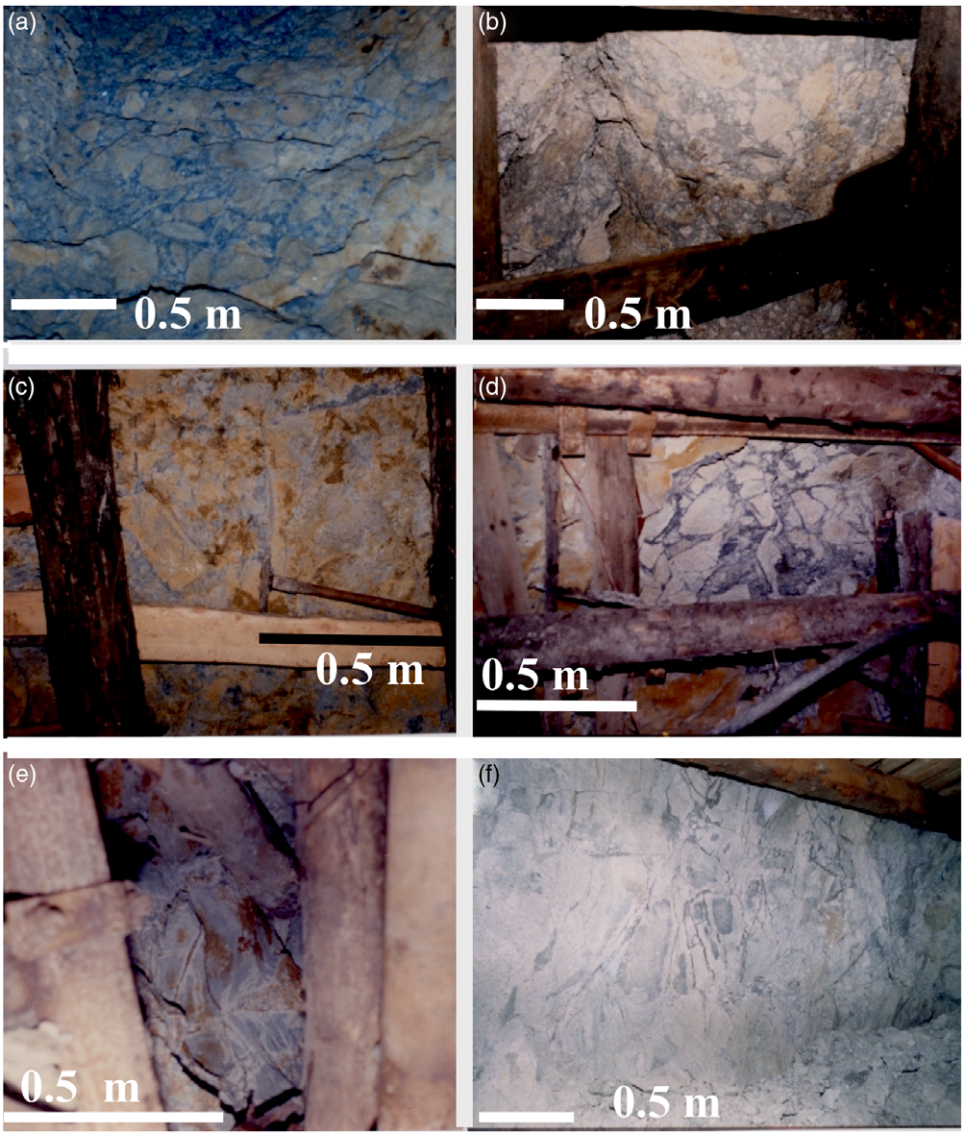

Fig. 3. (Colour online) Textural anatomy of the breccia structure: (a) Angular, sub-rounded and elliptical fragments of NH_4-I argillized andesite (15 to 50 cm) caught in a milled matrix (−30 m). (b) A chaotic texture with angular blocks and fragments (at the top) and smaller angular fragments in a flour-milled rock groundmass, where the breccia structure was cut by a fracture (−50 m). (c) The '*crample*' breccia texture with a '*shingle*' breccia texture (−80 m). (d) The '*jigsaw*' breccia texture (−90 m). (e) The '*crackle*' breccia texture (−110 m). (f) *In situ* hydraulic fracturing of andesite porphyry dyke (−110 m) and NH_4-I (5 %S) alteration where a tension and shearing fracture system is well highlighted. Reproduced (Fig. 3f) from Bobos & Eberl (2013) with permission of Springer Nature.

https://doi.org/10.1017/S0016756822000851 Published online by Cambridge University Press

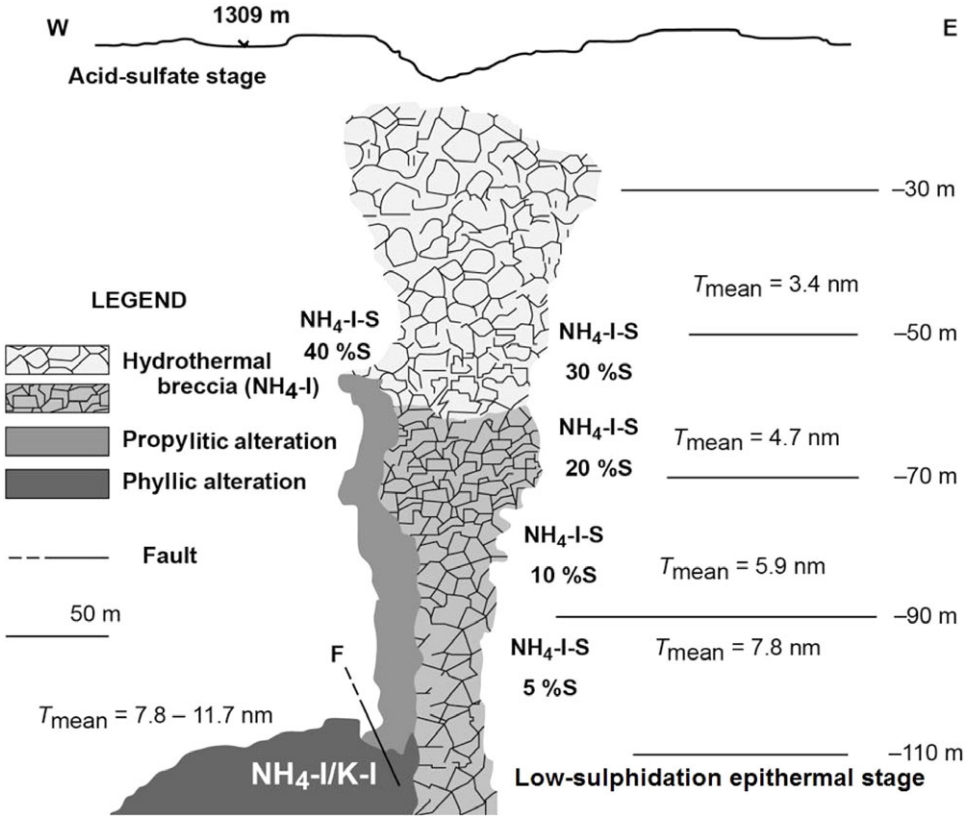

Fig. 4. The distribution of NH_4-I samples (taking into account the %S and T_{mean}) within the breccia structure (from −50 m to −110 m), and the relationship with K-I (phyllic) and propylitic alteration (after Bobos & Eberl, 2013). The breccia structure corresponds to fragments and blocks of andesitic flow that rose up by gas explosion (upper part) and fractured andesitic blocks *in situ* (bottom part). Reproduced from Bobos & Eberl (2013) with permission of Springer Nature.

a log-normal crystallite thickness distribution (CTD) shape. The T_{mean} of NH_4-I clays (<2 μm) increased with depth where a better correlation of NH_4-I–S with %S layers was found (Fig. 4). Two representative XRD patterns of NH_4-I–S mixed-layers with 5 and 30 % S, samples HB-18 (−90 m) and HB-4 (−55 m), are shown in Figure 5a, b.

The crystal growth of K-I and NH_4,K-I mixed clays collected from −110 m (outside the breccia structure) was also simulated, where two log-normal CTDs were identified corresponding to two different illite populations. Also, the T_{mean} of K-I ranges from 12.1 to 24.7 nm, higher than NH_4-I (e.g. <7.1 nm).

The NH_4 fixed in illite interlayers confirmed by Fourier transform infrared spectroscopy (FTIR) shows values of absorption bands characteristic of illite minerals (Fig. 6). Four absorption bands attributed to N–H stretching and bending are observed at 3340 cm^{-1}, 3040 cm^{-1}, 2840 cm^{-1} and 1430 cm^{-1}, with the absorption bands at 1430 cm^{-1} indicating the presence of NH_4^+ fixed in illite interlayers, corresponding to the fundamental vibration (ν_4) model for NH_4^+ (Petit *et al.* 2006).

The NH_4-I crystals show a variable morphology (Fig. 7) exhibiting randomly oriented lath-like aggregates with variable widths or platy aggregates.

4.d. Major-, trace- and rare earth element geochemistry

Major, trace and REEs were measured in K-I and NH_4-I altered andesite rocks collected from the breccia structure. The SiO_2 and Al_2O_3 contents measured in the NH_4-I altered rocks are ~60 % and 20 %, respectively (Table 1). High silica and low alumina contents were measured (Table 1) in the breccia cement, which are well correlated with the mineralogical data. A variable content of FeO was found in the whole rocks owing to the pyrite oxidation stage. Low amounts of MgO and CaO were found in the NH_4-I rich altered rocks. The content of H_2O increased as the smectite content increased in the illitic altered rocks.

The content of chalcophile elements (Cu, Pb, Zn, Bi, As, Ga, Sn) is generally lower in NH_4-I altered andesite (Table 2). The Cu, Pb, Zn and Bi amounts with high sulfur affinity show values below the geochemical clarke number of Cu (100 ppm), Pb (16 ppm) and Zn (50 ppm) as a limit of mineralization indicators. Ga ranges from 12.2 to 25.2 ppm and As from 6.2 to 13.4 ppm. Sn shows values from ~15 to 25 ppm in NH_4-I altered andesite. The siderophile elements (Co, Ni, W, Mo) show low values, where Mo is undetected in most of the samples or is close to the detection limit (2 ppm).

The light elements show high B and low Li concentrations (Table 2) in NH_4-I altered rocks. Also, a high amount of B was measured in illitic altered andesite samples close to fractured areas. Trace amounts of tourmaline in the assemblage with pyrite and quartz explain the presence of higher B amounts.

HFSEs (Nb, Ta, Zr, Hf, Y) show low concentrations close to those measured in fresh andesite rocks (Table 2). Low amounts of Nb (9 to 20 ppm) and Ta (0.2 to 0.8 ppm) were identified in NH_4-I altered rocks, where the Nb/Ta ratio ranges from 15.7 to 28.57 (fresh andesite rocks is ~53.33). In addition, the continental crust has a lower Nb/Ta ratio (= 12 to 13) than the bulk silicate Earth (Nb/Ta = 1479.3) (Münker *et al.* 2003). Zr ranges from 110 to 285 ppm and Hf from 3.9 to 7.4 ppm in the NH_4-I altered rocks. Lower values of Zr (55 ppm) and Hf (1.5 ppm) were measured in K-I/NH_4,K-I. The Zr/Hf ratio ranges from 20.37 to 55.12. The data plotted in the Nb versus Ta and Zr versus Hf diagrams do not show any fractionation between HFSEs.

Yttrium and Ho or Dy with a similar charge and size remained tightly coupled (Shannon, 1976) during the illitization process.

https://doi.org/10.1017/S0016756822000851 Published online by Cambridge University Press

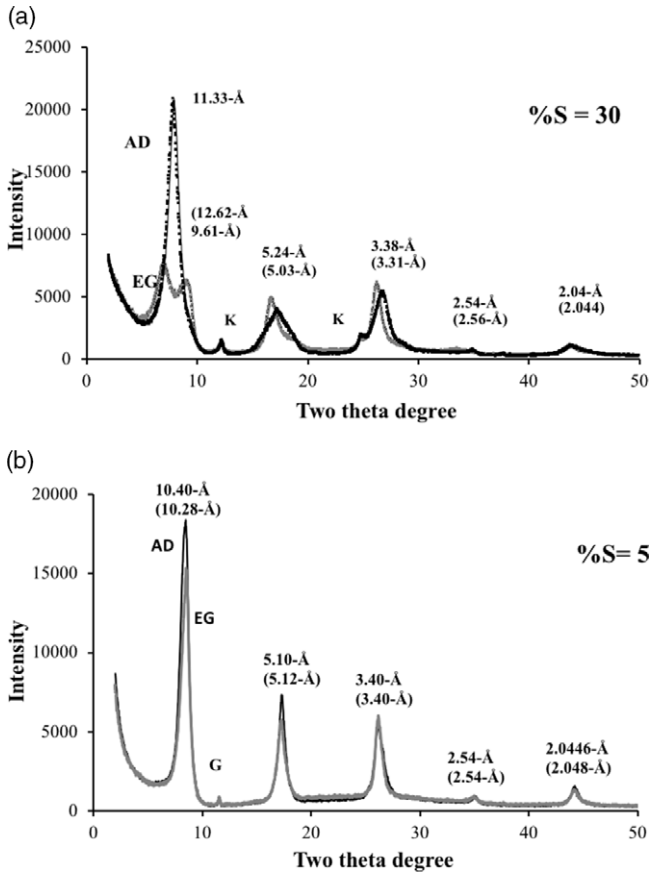

Fig. 5. Selected XRD patterns of NH_4-I–S ((a) 30 %S and (b) 5 %S) interstratified structure (<2 μm clay fraction) oriented specimens run in air-dried (AD) and ethylene glycol (EG) conditions using CuKα radiation. K – kaolinite; G – gypsum.

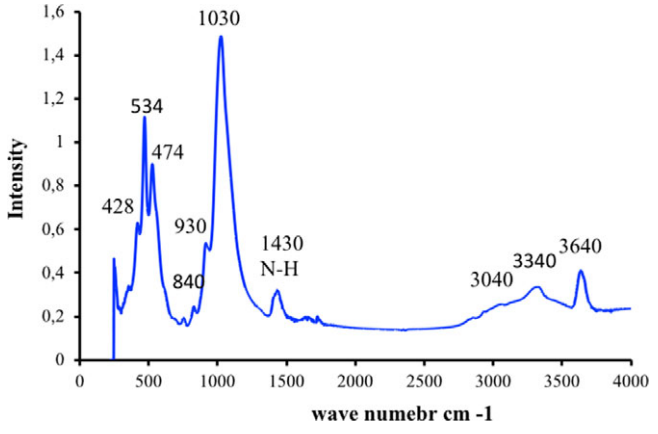

Fig. 6. (Colour online) Infrared spectrum of NH_4-I, indicating the NH_4 bending at 1430 cm^{-1}

Y ranges from 15 to 36 ppm, Ho from 0.62 to 1.16 ppm and Dy from 3.73 to 5.26 ppm. A very low correlation coefficient (not shown) was observed in the Y versus Ho and Y versus Dy diagrams. The Y/Ho ratio ranges from 16.30 to 46.15 and Y/Dy ratio from 3.10 to 8.99. The data plotted in the Y/Dy versus Y/Ho diagram show a moderate correlation coefficient (Fig. 8). By contrast, lower amounts of Y, Ho and Dy were measured in the K-I/NH_4,K-I altered andesite rocks than in the NH_4-I altered rocks.

Fig. 7. Scanning electron microscopy of NH_4-I crystals exhibiting a platy- and lath-shape morphology.

The CHArge-and-RAdius-Controlled (CHARAC) behaviour (Bau, 1996) of the element pairs Y–Ho and Zr–Hf was tested on fresh andesite, K-I/NH_4,K-I and NH_4-I altered andesitic rocks. In natural environments, Y and the REEs (with the exceptions of Ce and Eu) occur exclusively in the trivalent oxidation state, whereas Zr and Hf are tetravalent. In octahedral coordination, Y(III), Ho(III), Zr(IV) and Hf(IV) show close effective ionic radii of 1.019, 1.015, 0.84 and 0.83 Å, respectively (Shannon, 1976). The Y/Ho and Zr/Hf ratios of fresh andesite rocks, K-I/NH_4,K-I and NH_4-I altered rocks are close to the normalization ratios, indicating a CHARAC behaviour of these elements in silicate melts (Fig. 9).

The REE concentrations of whole argillic altered andesite rocks from the breccia structure are shown in Table 3. The ΣREE concentrations of NH_4-I and K-I/NH_4,K-I altered andesite rocks ranges from 104.25 to 135.96 ppm, where a higher amount of LREEs (85.05 to 111.62 ppm) than HREEs (5.33 to 7.96 ppm) characterize the NH_4-I altered rocks (Table 4). The La/Sm ratio is below unity (0.73–0.98), and the La/Yb ratio ranges from 0.46 to 0.89 (Table 4), where no correlation between La/Sm and La/Yb ratios was found.

The REE UCC normalization patterns of NH_4-I altered andesite rocks display a flat shape (Fig. 10), with a positive *Nd** anomaly from 1.22 to 1.69 and a slowly positive *Tm** anomaly ($Tm/Tm^* = (Tm_n)/(Er_n \times Yb_n)^{1/2}$) occurring. The ΣREE (56.14 ppm) of the K-I/NH_4,K-I sample is half of that in the NH_4-I samples, and a negative *Eu** anomaly (0.70) was identified (Table 4) by contrast with the UCC normalization pattern of the NH_4-I altered rocks.

4.e. Elemental analysis of volatile (C–N–H–S) and stable isotopes ($\delta^{13}C$ and $\delta^{18}O$)

The volatile (C–N–H–S) analysis was carried out either on the cement of breccia from open-space-filling, flour-rocks or argillic altered rocks (Table 5). Nitrogen is associated with carbon and other volatiles (i.e. H and S), where N (wt %) ranges from 0.143 to 1.231 and C wt % from 0.263 to 2.669 (Table 5). Both C and N were also measured for the <2 μm NH_4-I and K-I/NH_4,K-I

https://doi.org/10.1017/S0016756822000851 Published online by Cambridge University Press

Table 2. Traces and HFSE chemical elements of NH_4-I and K-I/NH_4,K-I argillic alteration of andesite rocks

Samples	Cu	Pb	Zn	Ag	Ga	Sn	Bi	Cr	Co	Ni	Sc	V	Zr	Nb	Hf	Ta	Th	U	Y	Sr	Ba	B	Mo
327	5	33	30	1	12	3	9	13	8	14	23	125	220	11	4.2	0.4	9	1.8	34	70	80	600	2
320	4	4	2	1	16	16	3.5	3	27	2	16	31	215	19	3.9	0.2	13	2.6	30	1.1	29	720	4
321	6	23	30	1	21	4	3	16	9	18	22	170	240	14	4.5	0.6	18	1.4	34	50	300	970	3
324	8	93	30	1	20	9	3	17	5	10	24	140	220	9	5.7	0.3	14	1.9	36	62	550	670	3
314	5.5	92	30	1	18.5	2	3	25	18	15	23	100	110	15	5.4	0.5	14	3.1	19	15	42	1250	3
352	6.5	100	36	1	25	5	3	7.5	7.5	3	13	155	155	14	6.7	0.7	12	2.8	21	15	500	620	3
211	25	2	43	1	17	16	3	25.5	15.5	17	21	140	145	10	4.9	0.4	16	1.7	15	18	61	710	2
340	4	13	44	2	19	13	7	15	7	10	14	150	110	11	5.3	0.7	18	2.6	15	54	360	1800	3
346	57	9	53	1	25	16	4.9	14	6	10	26	190	228	13	7.2	0.8	15	3.4	33	102	563	840	3
150	148	119	370	1	16	28	18.5	14	68	7.5	14	180	140	12	1.5	0.3	11	3.8	15	45	286	380	3
108a	122	27	156	1	25	15	18.5	16.5	33	13	25	212	285	20	7.4	0.7	13	3.1	25	120	736	935	3
Andesite	14	9.4	74	ndt	21	ndt	ndt	21	14.1	9	22	128	142	12.7	4.6	0.8	7.3	4.1	22.8	348	ndt	ndt	ndt

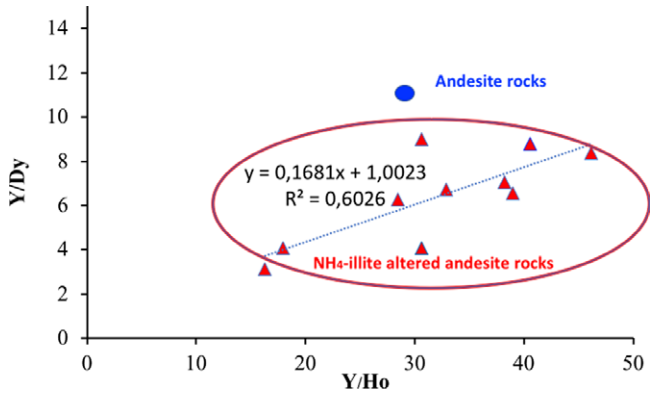

Fig. 8. (Colour online) Diagram of Y/Dy versus Y/Ho.

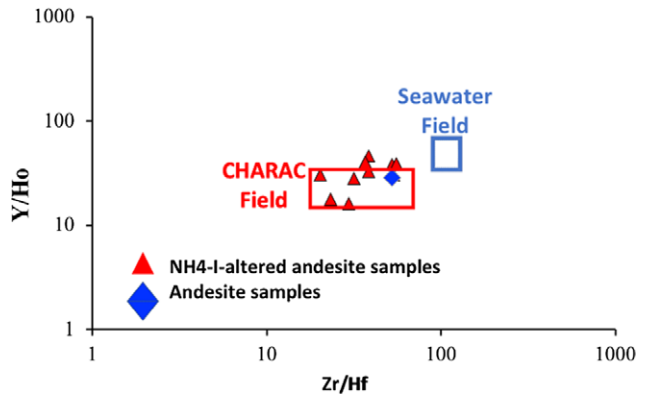

Fig. 9. (Colour online) Diagram of Y/Ho versus Zr/Hf (Bau, 1996) corresponding to altered and fresh andesite rocks.

fractions extracted from the argillized rocks. C (wt %) ranges from 0.20 to 0.66 and N (wt %) from 0.7 to 1.9 (Table 6). $\delta^{13}C$ (‰) ranges from −24.39 to −26.67 and $\delta^{15}N$ (‰) from 4.8 to 14.8 in the clay fractions (Table 6).

The $\delta^{18}O_Q$ isotope (V-SMOW) for quartz crystals collected from argillic andesite blocks at −110 m yielded a value at *c.* +15.12 ‰ (1τ), which represents a mean value of five samples. The $\delta^{18}O_F$ isotopic fractionation calculated for the quartz–H_2O pair (Clayton *et al.* 1972) is 7.73 ‰ (1τ) for the quartz precipitation at a temperature of 270–300 °C estimated from the fluid inclusion data (Guedes *et al.* 2000). Calculating $\Delta = \delta^{18}O_Q - \delta^{18}O_F$, a value of 7.39 ‰ (1τ) was obtained.

5. Discussion

5.a. Breccia architecture

The calc-alkaline plutons are multiphase in time and space, generating alteration–mineralization patterns centred on the intrusions, extending into a large volume of wall rocks from the top of the pluton (Sillitoe, 2010). Most plutons are characterized by multiple intrusive events with numerous porphyritic cupolas assumed to be connected at depth to a larger pluton.

The breccia structures described in the literature are associated with successive intrusive-tectonic stages, where a wide variety of positions in time and space may be represented within the porphyry systems (Sillitoe, 1985). Furthermore, the breccia structures are derived from an interaction of magmatic-hydrothermal–

https://doi.org/10.1017/S0016756822000851 Published online by Cambridge University Press

Table 3. REEs of NH_4-I and K-I/NH_4,K-I argillic alteration of andesite rocks

Samples	La	Ce	Pr	Nd	Sm	Eu	Gd	Tb	Dy	Ho	Er	Tm	Yb	Lu	Y
327	26.8	54.1	5.88	23.8	3.88	0.65	4.11	0.67	4.82	0.89	3.41	0.46	2.62	0.28	34
320	24.1	51.7	4.69	16.4	4.41	0.44	3.48	0.53	4.59	0.77	3.07	0.51	2.91	0.34	30
321	29.3	46.9	5.26	18.1	3.29	0.81	4.52	0.61	3.78	1.11	2.68	0.42	2.16	0.47	34
324	23.1	50.6	4.75	19.6	3.90	0.70	3.10	0.58	4.30	0.78	2.85	0.33	2.42	0.31	36
314	21.8	45.8	5.10	22.3	4.55	0.42	3.70	0.51	4.66	0.62	2.58	0.38	2.11	0.26	19
211	29.0	57.6	5.63	13.0	4.80	1.21	4.31	0.50	4.83	0.92	2.91	0.48	2.10	0.35	15
340	23.2	40.2	4.35	17.3	3.60	0.90	3.41	0.51	3.73	0.76	2.34	0.34	3.25	0.36	25
346	27.4	57.0	6.12	21.1	4.75	1.09	4.84	0.84	5.26	1.16	3.34	0.52	3.20	0.50	33
352	28.0	53.1	6.06	24.1	4.70	0.77	4.25	0.68	5.17	1.17	3.52	0.55	3.33	0.56	21
150	12.2	23.8	2.57	9.2	1.81	0.28	1.64	0.29	1.71	0.37	1.00	0.16	0.96	0.15	15

Table 4. Sum of the REE, LREE, MREE and HREE concentrations, the La/Sm and La/Yb UCC normalization ratios, the Eu* and Nd* anomalies and the ratios of Y/Ho and Y/Dy

Samples	SUMREE	LREE	MREE	HREE	$(La/Sm)_N$	$(La/Yb)_N$	Eu/Eu*	Nd/Nd*	Y/Ho	Y/Dy
327	132.37	110.58	15.02	6.77	1.05	0.66	0.71	1.69	38.20	7.05
320	117.94	96.89	14.22	6.83	0.83	0.53	0.49	1.22	38.96	6.53
321	119.41	99.56	14.12	5.73	1.35	0.87	0.91	1.48	30.63	8.99
324	117.32	98.05	13.36	5.91	0.90	0.62	0.87	1.55	46.15	8.37
314	114.79	95.00	14.46	5.33	0.73	0.67	0.44	1.57	30.64	4.08
211	127.64	105.23	16.57	5.84	0.92	0.89	1.15	0.85	16.30	3.11
340	104.25	85.05	12.91	6.29	0.98	0.46	1.11	1.48	32.89	6.70
346	137.12	111.62	17.94	7.56	0.87	0.55	0.99	1.33	28.44	6.27
352	135.96	111.26	16.74	7.96	0.90	0.54	0.75	1.53	17.95	4.06
150	56.14	47.77	6.10	2.27	1.02	0.82	0.70	1.45	40.54	8.77

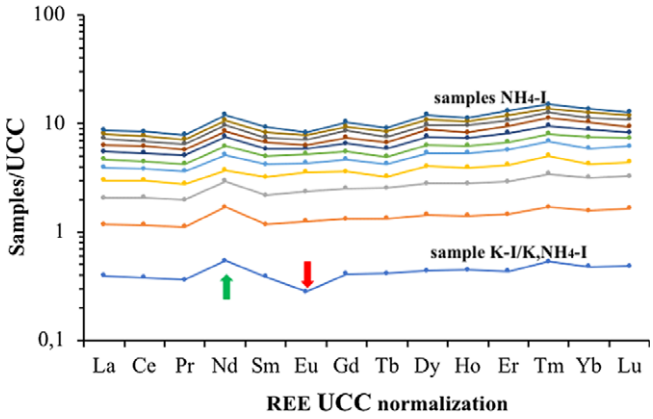

Fig. 10. (Colour online) The REE UCC normalization patterns of NH_4-I and K-I/NH_4,K-I argillic andesite rocks.

Table 5. The C–N–H–S volatile elements measured for NH_4-I and K-I/NH_4,K-I altered andesite rocks

Samples	C%	N%	H%	S%
327	0.263	0.146	0.429	0.009
320	2.669	0.143	0.716	0.035
321	0.345	0.152	0.648	0.028
324	0.319	0.162	0.736	0.014
314	0.734	0.167	0.686	0.024
211	0.492	0.382	0.761	0.048
352	0.388	0.493	0.748	0.077
340	0.416	0.810	0.716	0.244
346	0.439	1.231	0.891	0.821
150	0.330	0.548	0.805	16.89

structural–volcanic processes developed in an epithermal porphyry environment (Davies *et al.* 2000).

Subvolcanic intrusions located inside of the stratovolcano's edifices from the Neogene volcanic chain of the Eastern Carpathians (Gurghiu and Harghita) have generated a zonal hydrothermal alteration–mineralization pattern from potassic to phyllic, argillic and propylitic (Stanciu, 1984). Subvolcanic intrusive bodies of microdiorite to andesite composition generated the fossil hydrothermal system of Harghita Bãi, where the successive hydrothermal alteration stages (i.e. biotite, phyllic and argillic types) were probably associated with a porphyry copper system. The hydrothermal alteration stages previously described were identified in

https://doi.org/10.1017/S0016756822000851 Published online by Cambridge University Press

Table 6. The $\delta^{13}C$ and $\delta^{15}N$ isotope geochemistry of the <2 μm clay fractions of NH_4-I and K-I/NH_4,K-I samples extracted from the bulk altered argillized andesite

Samples[a]	Wt % N	$\delta^{15}N$[b]	Wt % C	Average	St_{dev}	$\delta^{13}C$ V-PDB	Ave	St_{dev}
	%	‰	%	%		‰	‰	‰
138430_1 (340)	1.9	**14.6**	0.54	0.53	0.01	**−26.73**	−26.67	0.08
138430_2	1.9	**14.8**	0.52			**−26.61**		
138431_1 (346)	1.4	**7.4**	0.65	0.65	0.01	**−24.43**	−24.39	0.05
138431_2	1.4	**7.3**	0.66			**−24.36**		
138443_1 (324)	1.6	**4.8**	0.20	0.21	0.01	**−25.18**	−25.49	0.44
138443_2	1.6	**4.8**	0.21			**−25.81**		
138426_1 (150)	0.7	**5.4**	0.38	0.38	0.004	**−25.75**	−25.78	0.05
138426_2	0.7	**5.4**	0.38			**−25.82**		

[a]The sample number corresponds to the <2 μm clay fractions and the number in parentheses corresponds to the whole altered rock discussed in this work.
[b]Data are from Bobos & Williams (2017).

several volcanic structures (i.e. Seaca-Tătarca, Ostoros, Mădăras) aligned along the NE–SW fracture system from the Gurghiu and Harghita mountains, being considered by Stanciu (1984) as similar to those alteration zones described for the Andean-type copper mineralization.

Furthermore, several types of breccia were described in the Neogene volcanic chain of the East Carpathians, such as: (i) the '*endogene*' breccia structures cemented by tuffaceous material in the eruptive structure of Zebrac-Mermezeu (South Călimani Mts) (Peltz *et al.* 1982*b*) or in the Seaca-Tătarca caldera (Gurghiu Mts) resulting from an '*unsuccessful*' volcanism (Peltz *et al.* 1982*a*); (ii) the hydrothermal breccia from the Ostoros caldera (Gurghiu Mts) interpreted as a '*metasomatic pseudobreccia*' (Stanciu, 1976); and (iii) the '*intrusive*' breccia from the Mădăras volcanic structure (north of the Harghita Mts) constituted by a '*chaotic*' distribution of sedimentary (i.e. pelitic rocks), well-rounded quartz grains and volcanic rocks (Stanciu *et al.* 1984). In most cases, the hydrothermal breccias from the Neogene volcanism of the Carpathians are blind mineralized structures.

In fact, larger meteoric–hydrothermal breccia structures in porphyry-Cu systems resulting from flashing of relatively cool ground waters on approach to magma are usually related to late-mineral porphyry dykes, which may display a downward transition to porphyry intrusions (Sillitoe, 2010). The intrusion size controls the longevity of intrusion-induced hydrothermal circulation and heat transfer, which may or may not make long-lasting hydrothermal systems.

In the VHB volcanic structure, a conductive magmatic-hydrothermal circulation generated a suite of hydrothermal alterations from potassic (biotite) to phyllic (K-I) and to argillic and advanced argillic alteration. The breccia structure described in the Harghita Băi hydrothermal area resulted from hydro-fracturing of the installed porphyry intrusive dyke owing to a high-pressure hydrothermal fluid circulation within the evolution of a magmatic-hydrothermal system. Also, crustal fracturing played a main role regarding the porphyry intrusive dyke installation, where the breccia structure displays a net-like contact at different underground levels with the NE–SW crustal fracture. The rocks interacted with water-rich hydrothermal solutions at a high fluid pressure within the fissures and fractures and then, the effective pressure decreased subsequently leading to fracture propagation along the breccia structure (Sibson, 1977, 1986; Laznicka, 1988; Scholz, 1990; Jebrak, 1997; Taylor & Pollard, 1993).

The fragment geometry (e.g. morphology and distribution) may be a key mechanism for the brecciation process, with the initially *in situ* '*crackle*' propagation event being observed from −110 m to −80 m. After this, the effect of high gas pressure facilitated the splaying of wall rock into angular rock fragments cemented by a fine quartz-rich andesite material. The following sequences were recognized, e.g. initial fracturing of andesite, degassing of volatiles, collapse and diffusion of hydrothermal fluids across open spaces. The breccia structure architecture and mineralogical composition are characterized by the following elements: (i) *in situ* fracturing of andesitic rocks ('*crackle*'); (ii) fragmentation ('*shingle*') and explosion of andesitic rocks at the top of the breccia structure; (iii) transported fragments (e.g. clasts) which favoured the permeability increases; (iv) open spaces filled with fine materials resulting from fracturing; and (v) K-I alteration outside the breccia structure and NH_4-I alteration within the breccia structure. No contact between the intrusion breccias and the altered porphyry intrusive dyke was identified.

In addition, a tension and shearing fissure system observed in the brecciated altered andesite dyke (Fig. 3f) follows the breccia structure formation, probably related to the last volcanic eruption.

5.b. Mineralogy and geochemistry

Impregnation of the andesite (formation of impregnated texture) and hydrothermal alteration stages (illitization in the presence of NH_4) from the brecciated structure were related to a complex of hydrothermal events, with various geological and physical factors being responsible for their formation. Among these factors are the andesite dyke emplacements, brecciation-types, permeability and the origin of the hydrothermal fluid. In addition, the fluid chemistry may be varied or not provide trace elements that represent an important fingerprint of the fluid origin.

The breccia structure devoid of ore is a peripheral injection breccia formed during the VHB stratovolcano evolution, where the andesite blocks supported a low-sulfidation-type alteration (Hedenquist & Lowenstern, 1994) or a phyllic and argillic alteration (Meyer & Hemley, 1967). Another aspect previously discussed (Bobos & Williams, 2017 and references therein) emphasized the mineralogy, geochemistry and fluid chemistry. Mineralogical data obtained on clay fractions extracted from argillic altered andesite identified a series of NH_4-I–S mixed-layered clays (see Fig. 4)

https://doi.org/10.1017/S0016756822000851 Published online by Cambridge University Press

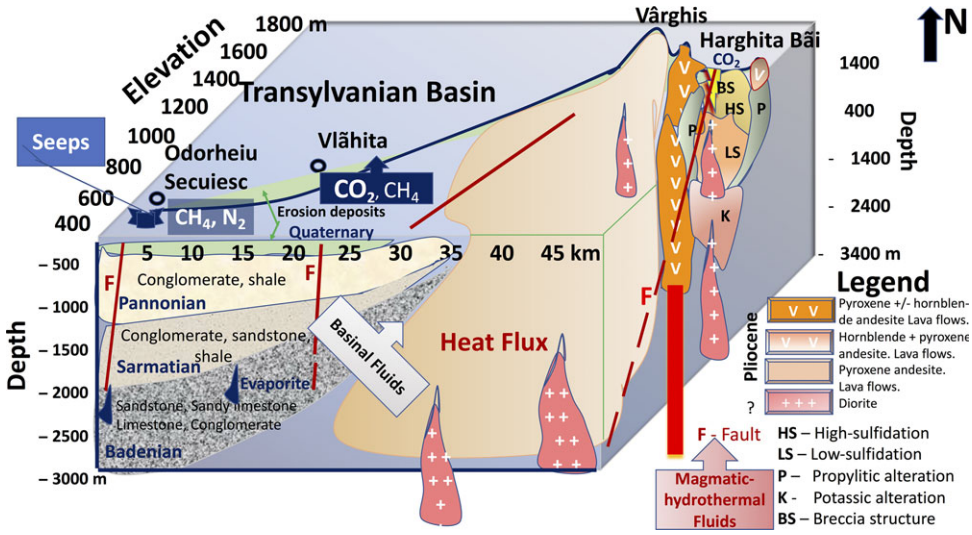

Fig. 11. (Colour online) Suggested sketch of volcano–basement interaction and the geological transect profile (see Fig. 1c) from Odorheiu Secuiesc to the Vârghis–Harghita Băi stratovolcano with expelled seeps, mud, CO_2-free spring discharge and basinal fluids (C and N) along the permeable zones from the boundary between the Transylvanian basin basement and the Harghita volcanic arc.

within the breccia structure, and K-I + NH_4,K-I mixed phases outside of the breccia structure (−110 m).

The illite reaction history in the Harghita Băi hydrothermal system was obtained by studying the evolution of the shapes of their CTDs where different isotope ratios were preserved during the illite crystal growth mechanisms (Williams & Hervig, 2006). The NH_4–I–S mixed layer distribution within the breccia structure reflects variations of %S and T_{mean} as fracturing degree and temperature decreased in the breccia structure from −110 m to −30 m (see Figs 3, 4; Bobos & Eberl, 2013). Therefore, NH_4–I crystals grew up to 7.8 nm (5 %S), whereas K–I crystals grew larger, up to 24.7 nm. Also, light isotopes ($\delta^{11}B$ and $\delta^{7}Li$) previously measured on the K-I and NH_4-I–S series confirmed different fluid sources in the crystallization of illite crystals (Bobos & Williams, 2017).

Furthermore, HFSE and REE geochemistry provide important insights into the water–rock interaction where the relative abundances of these elements depend upon the temperature, fluid chemistry, pH and type of altered rock. The concentrations of HFSEs measured on NH_4-I altered rocks show low concentrations below reported values in fresh andesite rocks (Nb = 15–20 ppm; Ta <0.6 ppm; Zr = 160–240 ppm). The geochemical behaviour of Nb and Ta is intimately linked to abundant Ti in oxide minerals, where Fe–Ti oxides (i.e. rutile and ilmenite) are the dominant host minerals of Ti, Nb and Ta in crustal rocks. The Nb/Ta ratio (15.71 to 28.57) in the NH_4-I argillic altered rocks is lower than in fresh andesite rocks (>53.3). Given that amphibole favours Nb over Ta, the fluids in equilibrium with amphibole should have low Nb/Ta. A slight increase in Zr is observed in the NH_4-I altered rocks, where the Zr/Hf ratio shows a large fractionation from 39.74 to 102.38. This is explained by the breakdown of pyroxene and amphibole, which released Zr into the hydrothermal fluids, resulting in Zr gains by the hydrothermally altered rocks (Rubin *et al.* 1993).

Lower concentrations of Y, Ho and Dy were found in the NH_4-I altered andesite samples than the fresh andesite rocks. The Y/Ho ratios represent a geochemical proxy indicative of the water–rock interaction and adsorption processes by clays. The Y/Ho ratio (16.30 to 46.15) is below the chondritic molar ratio (continental crust) of 52 (McDonough & Sun, 1995). The Y/Ho ratio variations are well explained through the formation of alteration minerals, which in turn may induce different scavenging effects on these elements (Bau, 1999). By contrast, an elevated Y/Ho ratio (~101) in hydrothermal fluids corresponds to mixing with seawater (Bau & Dulski, 1995; Bau *et al.* 1997). The lower Y/Ho ratio measured and lack of a Ce* anomaly in our samples suggests that the hydrothermal fluid was not mixed with seawater. The Y/Dy ratio (3.10 to 8.99) also shows low values close to those values corresponding to andesite rocks.

The Y/Ho and Zr/Hf ratios were used to verify whether Y, REEs, Zr and Hf in the argillic altered rocks were inherited from the andesite rocks or aqueous fluids. Fresh andesite igneous rocks and NH_4-I altered andesitic rocks show Y/Ho and Zr/Hf ratios close to the chondritic ratios (Fig. 9), indicating a CHARAC behaviour of these elements in silicate melts. The Y/Ho and Zr/Hf ratios reflect their source rocks, confirming no contribution of aqueous solutions to the NH_4-I andesite alteration.

Seawater (e.g. natural low-temperature aqueous solution) is characterized by Y/Ho ratios between 44 and 74 and by Zr/Hf ratios between 85 and 130 (Zhang *et al.* 1994; Bau *et al.* 1995). The Zr/Hf ratio is considerably higher than those values suggested by Boswell & Elderfield (1988).

The REE normalized patterns of the K-I/NH_4,K-I and NH_4-I altered andesite reflect two different fluids during illite mineral crystallization in two distinct K–Ar dated events (Clauer *et al.* 2010). The REE data obtained on the NH_4-I altered andesite rocks series (Tables 3, 4) show a fractionation trend with a positive *Nd** anomaly and no *Eu** anomaly relative to UCC normalization by contrast with the K-I/NH_4,K-I altered andesite rocks which show a negative *Eu** anomaly (Fig. 11). The positive *Nd** anomaly relative to UCC identified in the NH_4-I altered andesite was not inherited from the andesite rocks, indicating a boundary exchange process derived from another fluid composition generated by an external source (i.e. organic influences, basinal fluid). Also, the slight increase of the *Tm** anomaly could reflect the influence of tourmaline (reflecting Tm-bearing minerals) in the NH_4-I altered andesitic rocks.

Preliminary fluid inclusion data identified four primary coeval types (aqueous one-phase (L), aqueous two-phase (L–V), rare aqueous multiphase (L–V–S) with a halite cube and carbonic one-phase (V) at room temperature in the NaCl–$CaCl_2$–$MgCl_2$–H_2O–(CH_4–CO_2) system) in small quartz crystals grown in the argillic mass of the NH_4-I altered andesite (−110 m), where the coexistence of H_2O–$CaCl_2$($MgCl_2$)–NaCl brines and CH_4-vapours in fluid inclusions resulted from an immiscibility process at a

https://doi.org/10.1017/S0016756822000851 Published online by Cambridge University Press

temperature of 270 °C and pressure of 100 MPa, respectively (Guedes *et al.* 2000). The CH_4 identified as vapours in fluid inclusions derived from a variety of carbon host-rock sources from the Transylvanian basin. Probably, the CH_4 was associated with other major gases (e.g. CO_2, N_2, H_2O, etc.) in the initial stage, where individual gases were fractionated later into vapour phases (Giggenbach, 1980).

Furthermore, high amounts of organic carbon and nitrogen were measured either in whole rocks or the <2 μm clay fractions (Tables 5, 6). The $\delta^{13}C$ measured is strongly depleted (−24.39 to −26.67 ‰) in the NH_4-I–S clay fractions (<2 μm), reflecting values close to oxidation of thermogenic CH_4, which typically indicates a moderate level of $\delta^{13}C$-depletion (−20 to −50 ‰) (Whiticar, 1999). The $\delta^{13}C$ values obtained are different to those measured in the CO_2-free springs discharged from the Harghita Băi area, which round to −4.21 ‰ (Vaselli *et al.* 2002), but are very close to those values for gas seeps from the small Homorod mud volcano ($\delta^{13}C = -25.68$ ‰, Homorod 3, eastern Transylvania basin border with the Neogene volcanic arc; see Fig. 1b), where extremely high concentrations of nitrogen (>92 vol. %) and helium (up to 1.4 vol. %) were measured (Etiope *et al.* 2011).

$\delta^{15}N$ (‰) ranges from +4.8 to +7.4 (± 0.6) for the NH_4-I–S and NH_4,K-I clays, with one outlier for NH_4-I–S of +14.6 (± 0.6) (Bobos & Williams, 2017), which supports the interpretation of an influx of waters from organic sediment ($\delta^{15}N \geq +5$ ‰). Also, such high positive $\delta^{15}N$ values acquired by the NH_4-I–S (5 %) clays have been observed in the presence of meteoric waters mixed with hydrothermal fluids (Haendal *et al.* 1986). Nitrogen in both types of NH_4-I–S and NH_4,K-I mixed-layered clays from the Harghita Băi area is attributable to shales of Miocene age from the Transylvania basin, since the major fraction of coexisting carbon is derived from the same source (Sano & Williams, 1996).

5.c. Boundary fluid exchange: isotopic records

Fluid–rock interaction is an exchange of elements taking place at increasing temperatures, where the interaction involves dissolution–precipitation, chemical exchange reactions, redox reactions, diffusion and their combinations.

Oxygen isotopes measured on neoformed bipyramidal quartz crystals collected from argillic '*crackle*' andesite rocks at −110 m yielded a value of 15.12 ‰ (1τ) in equilibrium with a calculated $\delta^{18}O_F$ value of 7.73 ‰ (1τ), corresponding to waters with a magmatic isotopic composition. Light isotopes ($\delta^{11}B$ and $\delta^{7}Li$) measured previously for the K-I/NH_4,K-I mixed clays correspond to a magmatic fluid enriched in heavy-B and Li (Bobos & Williams, 2017). This is well supported by $\delta^{18}O$ isotope data obtained on neoformed quartz crystals, which confirmed the presence of a magmatic-hydrothermal fluid circulation which generated the hydrothermal system probably earlier than 9.5 Ma, the absolute age of K-I alteration identified at −110 m outside of the breccia structure. By contrast, the NH_4-I–S series is consistent with an influx of isotopically light-B and Li waters ($\delta^{11}B = -12$ to -22.4 ± 0.8 ‰; $\delta^{7}Li = -8.6$ to -12.3 ± 0.8 ‰) derived from hydrothermal leaching of continental evaporite and/or organic-rich sediments (Bobos & Williams, 2017). This is also supported by $\delta^{13}C$ isotope data (−26 ‰) obtained on clay fractions which show values close to those values from macro- or microseepage gas observed in the eastern margin of the Transylvanian basin (i.e. Praid, Odorheiu Secuiesc, Homorod) related to thermogenic reservoirs in tectonically active areas (Etiope *et al.* 2011), where the $\delta^{13}C$ of released gas ranges from −25 to −45 ‰ (Klusman *et al.* 2000).

The HFSEs measured on both the K-I/NH_4,K-I and NH_4-I altered rocks were inherited from the source rocks, indicated also by the CHARAC behaviour of these elements (Fig. 9). Otherwise, the REE patterns show differences between the K-I/NH_4,K-I and NH_4-I samples with respect to *Eu** and *Nd** anomalies, indicating fluid changes with respect to NH_4-I alteration. The negative *Eu** anomaly of K-I/NH_4,K-I suggests a partial breakdown of plagioclase from andesite rocks. Different fluid sources with no *Eu** anomaly and *Nd** anomaly correspond to the NH_4-I altered rocks.

5.d. A proposed model of non-magmatic fluid circulation, origin and trap

The argillic alteration areas in a continental volcanic arc are an important key in understanding the origin of the fluids involved in hydrothermal systems, with the K-I and NH_4-I clays from the Harghita Băi hydrothermal system retaining magmatic and non-magmatic signatures. The geochemical signatures serve as a tracer of the mobility of magmatic and organic–sedimentary components in the upper continental crust. Physical and chemical interactions between the host rock and migrating fluids profoundly affect elemental geochemical cycling among seawater, sediments, crust and mantle reservoirs (Moore & Vrolijk, 1992).

The presence of mud volcanoes and seepage across the back-arc continental '*sag*' basin of Transylvania (Tiliță *et al.* 2013, 2015) resulted from active compressional tectonics perturbing deep natural gas and petroleum reservoirs, where the Neogene volcanism (from Late Miocene to Quaternary times) caused a heat flow increase and simultaneous basin uplift, reaching temperatures of 200 °C at depths shallower than 3000 m, where most gas reservoirs are located in the eastern Transylvania basin margin (Krézsek *et al.* 2010). The gas structures close to the Neogene volcanic chain contain higher concentrations of CO_2 (up to 90 %), N_2 (up to 60 %) and He (up to 5 %) (Filipescu & Huma, 1979).

Peripheral deformation of the pre-volcanic shallow sedimentary basement of the eastern part of the Transylvanian basin induced sagging and spreading of the nearby large volcanic edifices as well as enhanced the salt diapirism owing to the effect of increased heat-flux (Tiliță *et al.* 2013). The post-salt succession tilting is related to salt withdrawal processes and rotation of the whole post-salt sedimentary succession along the salt-layer acting as a detachment surface (Szakács & Krézsek, 2006).

The igneous calc-alkaline intrusions increased the temperature, sufficient for catagenesis of the rocks from the eastern margin of the Transylvanian basin, which was accompanied by abrupt overpressure and host-rock fracturing, which favour organic fluid expulsion (Schutter, 2003*b*; Iyer *et al.* 2017). The Praid, Corund, Morareni, Odorheiu Secuiesc and Homorod seeps and volcanic muds (Fig. 11) expelled both biogenic and thermogenic methane along the anticlinal structures, faults related to salt diapirism or fractures on the eastern margin of the Transylvanian basin (Etiope *et al.* 2011; Italiano *et al.* 2017), where most seeps are linked to gas reservoirs (Baciu *et al.* 2018). Such transitional sedimentary versus magmatic systems (Fig. 11) implied the temperature increases around the reservoir, abrupt overpressure, host-rock fracturing and the expulsion of organic fluid with a chemical composition that reflected the host rocks: CH_4, N_2, B, Li, salts and water (based on fluid inclusion data on quartz and the light isotope composition of NH_4-I clays).

Migration along faults or fractures of dissolved gases in thermal springs or groundwater is well highlighted across the transect profile from Odorheiu Secuiesc and Vlăhita to the Harghita Băi area

https://doi.org/10.1017/S0016756822000851 Published online by Cambridge University Press

(Fig. 11). Here, CO_2 rises during subsurface gas–water interactions between the pristine air-equilibrated water (normally infiltrating as air saturated water; ASW) and deep-seated endogenic gases of variable origin (organic, crustal and/or mantle-derived) (Vaselli *et al.* 2002; Italiano *et al.* 2017).

The post-intrusive fracture system (NE–SW) recognized in the CGH volcanic chain (Szakacs & Seghedi, 1995) opened the circulation routes for volatile escape during the consolidation of the intrusive bodies. Late volcanic activity dated from 6.5 to 3.9 Ma (Pecskay *et al.* 1995) in the northern part of Harghita opened or reactivated new pathways and provided new circulation routes for basinal fluids from the petroleum system of the eastern Transylvanian basin to new and old permeable zones (faults, breccia structures, etc.) and expelled seeps from the biogenic petroleum system of the Transylvanian basin.

The presence of gas accumulations with high concentrations of CO_2 (up to 90 wt %) and N_2 (up to 40 wt %) typify gas fields in the close proximity of the Pliocene volcanic rocks at the southeastern borders of the basin that provided additional heat and gases to the hydrocarbon system (Paraschiv, 1980; Krézsek *et al.* 2010). Both carbon and nitrogen from various organic sediments from the Transylvanian basin were transferred in the volcanic continental arc and then, N was fixed as NH_4^+ into illite clays, reflecting a complete palaeo-biogeochemical cycle. Pyrolysis experiments suggest that N_2-rich gas is released during the final stage of gas generation, after CH_4 formation has ceased (Krooss *et al.* 1995). Values of $+4\ ‰ > \delta^{15}N < +18\ ‰$ imply that the N_2 may have originated from post-mature sedimentary organic matter (Zhu *et al.* 2000).

The K–Ar age of 9.5 ± 0.5 Ma obtained for K-I confirmed an early post-magmatic stage related to an early magmatism with implications probably at deep depths for thermogenic gas generation. The time of dry-gas generation from the post-salt sediments or biogenic petroleum system (Mid- to Late Miocene), estimated to be 7–9 Ma (Ciulavu *et al.* 2000), is older than the last volcanism event dated from 6.3 to 3.9 Ma (Peltz *et al.* 1987; Pecskay *et al.* 1995) corresponding to the intermediate zone of the VHB stratovolcanic structure. This agrees also with the K–Ar data (<6.2 ± 0.6 Ma) previously obtained on the NH_4-I alteration event (Clauer *et al.* 2010), where basinal fluids transported the organic elements from the biogenic petroleum system. The absolute ages obtained on the NH_4-I alteration correlated with the absolute ages of the last volcanism, suggesting that the dry-gas generation from the post-salt sediments began before 6.3 Ma.

6. Conclusion

The thermal influence of the shallowest-level diorite intrusions resulted in abrupt expulsion of magmatic-hydrothermal fluids, which generated potassic (biotite), phyllic (K-I, 9.5 Ma) and argillic alteration. The hydrothermal injection breccia may be indicative of abrupt overpressure build-up and magmatic-hydrothermal fluid expulsion during this first hydrothermal event. Several evolution stages of brecciation were recognized by textural aspects identified from top to bottom, such as: '*shingle*', '*jigsaw*', '*crackle*' and hydraulic *in situ* fracturing.

The second hydrothermal event related to basinal fluid (organic) circulation in the Harghita Băi hydrothermal system occurred after the last volcanic activity, where several younger late-stage andesitic lava extrusions (e.g. Harghita Ciceu, Borhegy, etc.) appeared and obtruded the older cratered areas of the VHB stratovolcano. The last volcanism (6.3 to 3.9 Ma) and simultaneous volcano-induced tectonic activity in the proximity of the eastern Transylvanian basin basement increased the heat flow, generating lateral salt extrusion, basin uplift, enhanced diapirism and pressure increase in the gas reservoir. The basinal fluid with a chemical composition reflecting the host – post-salt petroleum system – (CO_2, CH_4, N_2, salts, B, Li and water) expelled seeps, mud pools and organic fluids in the vicinity of the volcanic continental arc (e.g. Praid, Odorheiu Secuiesc, etc.), where basinal fluids circulated along permeable zones (i.e. fractures, faults) and interacted within the stratovolcanic structures of the Harghita Mts.

The HFSE behaviours of the K-I and NH_4-I argillic altered andesite are close to chondritic ratios, indicating no contribution of hydrothermal fluid, especially on NH_4-I andesite alteration and the CHARAC behaviour within silicate melts. Nevertheless, REE normalized patterns show two distinct trends, one with a *Eu** anomaly (K-I) and the other with a *Nd** anomaly (NH_4-I), indicating a boundary exchange with the organic-enriched waters. The strongly depleted $\delta^{13}C$ (V-PDB) measured in the NH_4–I clays shows values (−24.39 to −26.67 ‰) close to CH_4 thermogenic oxidation, whereas the $\delta^{15}N$ confirmed that the N_2 originated from post-mature sedimentary organic matter. The phyllic alteration (K-I) related to an early magmatic-hydrothermal event identified in the fossil hydrothermal system of Harghita Băi was later replaced by NH_4-I alteration owing to circulation of the organic-rich fluid along permeable zones after the breccia pipe formation.

Acknowledgements. I thank Prof. Ioan Mârza from the 'Babes-Bolyai' University of Cluj-Napoca (Romania) who kindly accompanied me on the field trip in the Harghita Băi area. I acknowledge use of the Keck Environmental Lab assisted by Natalya Zolotova from the Arizona State University (USA). I thank Dr Henrik H. Svensen (Univ. Oslo) for review that greatly improved the earlier version of the manuscript. Also, I am very grateful to Prof. Lynda B. Williams (ASU-Tempe, USA) for through reading and comments and to Dr Tim Johnson (editor) for excellent editorial handling. In addition, I acknowledge Paolo Fulignati (Pisa University, Italy) for the reading and suggestions.

References

Allman-Ward P, Halls H, Rankin A and Bristow CM (1982) An intrusive hydrothermal breccia body at Wheal Remfry in the western part of the St. Austell granite pluton, Cornwall, England. In *Mineralization Associated with Acid Magmatism* (ed. AM Evans), pp. 1–28. Chichester: John Wiley & Sons.

Baciu C, Ionescu A and Etiope G (2018) Hydrocarbon seeps in Romania: gas origin and release to the atmosphere. *Marine and Petroleum Geology* **89**, 130–43.

Bau M (1996) Controls on the fractionation of isovalent trace elements in magmatic and aqueous systems: evidence from Y/Ho, Zr/Hf, and lanthanide tetrad effect. *Contributions to Mineralogy and Petrology* **123**, 323–33. doi: 10.1016/S0377-0273(98)00117-6.

Bau M (1999) Scavenging of dissolved yttrium and rare earths by precipitating iron oxy-hydroxide: experimental evidence for Ce oxidation, Y/Ho fractionation, and lanthanide tetrad effect. *Geochimica et Cosmochimica Acta* **63**, 67–77.

Bau M and Dulski P (1995) Comparative study of yttrium and rare-earth element behaviours in fluorine-rich hydrothermal fluids. *Contributions to Mineralogy and Petrology* **119**, 213–23.

Bau M, Dulski P and Muller P (1995) Yttrium and holmium in South Pacific seawater: vertical distribution and possible fractionation mechanisms. *Chemie der Erde* **55**, 1–15.

Bau M, Moller P and Dulski P (1997) Yttrium and lanthanides in eastern Mediterranean seawater and their fractionation during redox cycling. *Marine Chemistry* **56**, 123–31.

Bobos I (2012) Characterization of smectite to NH4-illite conversion series in the fossil hydrothermal system of Harghita Bai, East Carpathians, Romania. *American Mineralogist* **97**, 962–982.

https://doi.org/10.1017/S0016756822000851 Published online by Cambridge University Press

Bobos I (2019) Nanoscale coexisting phases of K-I and NH_4K-I, and NH_4-I-S clays: an organic nitrogen contribution in the Harghita Băi, E-Carpathians, Romania. *Clay Minerals* **54**, 27–40.

Bobos I and Eberl DD (2013) Thickness distributions and evolution of growth mechanisms of NH_4-illite from the fossil hydrothermal system of Harghita Băi, Eastern Carpathians, Romania. *Clays and Clay Minerals* **61**, 375–391.

Bobos I and Ghergari L (1999) Conversion of smectite to ammonium illite in the hydrothermal system of Harghita Băi, Romania: SEM and TEM investigations. *Geologica Carpathica* **50**, 379–387.

Bobos I and Williams LB (2017) Boron, lithium and nitrogen isotope geochemistry of NH_4-illite clays in the fossil hydrothermal system of Harghita Băi, East Carpathians, Romania. *Chemical Geology* **473**, 22–39.

Boswell SM and Elderfield H (1988) The determination of zirconium and hafnium in natural waters by isotope dilution mass spectrometry. *Marine Chemistry* **25**, 197–209.

Ciulavu D, Dinu C, Szakács A and Dordea D (2000) Late Miocene to Pliocene kinematics of the Transylvania basin. *American Association of Petroleum Geologists Bulletin* **84**, 1589–615.

Clauer N, Liewig N and Bobos I (2010) K-Ar, $\delta^{18}O$ and REE constraints on the genesis of ammonium-illite from the Harghita Băi hydrothermal system, Romania. *Clay Minerals* **45**, 393–411.

Clayton RN and Mayeda TK (1963) The use of bromine pentafluoride in the extraction of oxygen from oxides and silicates for isotopic analysis. *Geochimica et Cosmochimica Acta* **27**, 43–52.

Clayton RN, O'Neil JR and Mayeda TK (1972) Oxygen isotope exchange between quartz and water. *Journal of Geophysical Research* **77**, 3057–67. doi: 10.1029/JB077i017p03057.

Corbett GJ and Leach TM (1998) *S.W. Pacific Rim Au/Cu Systems: Structure, Alteration and Mineralization*. Society of Economic Geologists, Special Publication no. 6. doi: 10.5382/SP.06.

Craciun P and Bandrabur T (1993) Some hydrogeochemical features of the geothermal areas related to the Neogene volcanics in the Harghita Mountains, Romania. *Bulletin AHRZ* **2**, 11–19.

Craig A (1953) The geochemistry of the stable carbon isotopes. *Geochimica et Cosmochimica Acta* **3**, 53–92.

Davies AGS, Cooke DR and Gemmell BJ (2000) Breccias associated with epithermal and porphyry systems towards a systematic approach to their description and interpretation. In *Gold in 2000: Poster Session Extended Abstracts, Lake Tahoe, Nevada, November 10–11, 2000* (eds LA Bucci and JL Mair), pp. 98–103.

Eberl DD, Drits VA and Środoń J (1998) Deducing crystal growth mechanisms for minerals from the shapes of crystal size distributions. *American Journal of Science* **298**, 499–533.

Etiope G, Baciu C and Schoell M (2011) Extreme methane deuterium, nitrogen and helium enrichment in natural gas from Homorod seep (Romania). *Chemical Geology* **280**, 89–96.

Feng ZQ (2008) Volcanic rocks as prolific gas reservoir: a case study from the Qingshen gas field in the Songliao Basin, NE China. *Marine and Petroleum Geology* **25**, 416–32.

Fielitz W and Seghedi I (2005) Late Miocene–Quaternary volcanism, tectonics and drainage system evolution in the East Carpathians, Romania. *Tectonophysics* **410**, 111–36.

Filipescu MN and Huma I (1979) *Geochimia Gazelor Naturale (Geochemistry of Natural Gases)*. Bucuresti: Editura Academiei, 175 pp. (in Romanian).

Giggenbach WF (1980) Geothermal gas equilibria. *Geochimica et Cosmochimica Acta* **45**, 393–410.

Goldfarb RJ, Baker T, Dubé B, Groves DI, Hart CJR and Gosselin P (2005) Distribution character and genesis of gold deposits in metamorphic terranes. *Economic Geology: One Hundredth Anniversary Volume* (JW Hedenquist, JFH Thompson, RJ Goldfarb and JP Richards), pp. 407–50. Littleton: Society of Economic Geologists.

Goode AJJ and Taylor RT (1980) *Intrusive and Pneumatolytic Breccias in South-west England*. Institute of Geological Sciences Report vol. 80/2. London: H.M. Stationary Office.

Gries RR, Clayton JL and Leonard C (1997) Geology, thermal maturation, and source rock geochemistry in a volcanic covered basin: San Juan Sag, south-central Colorado. *American Association of Petroleum Geologists Bulletin* **81**, 1133–60.

Guedes A, Bobos I, Liewig N and Noronha F (2000) Fluid inclusion and oxygen isotope analyses on quartz related to tobelitic environment from the Harghita Băi, East Carpathians, Romania. In *ECROFI Abstract Book* (eds F Noronha, A Doria and A Guedes), pp. 46–9. Faculdade de Ciencias do Porto, Departamento de Geologia, Memoria vol. 7.

Haendel D, Muhle K, Nitzsche H-M, Stiehl G and Wand U (1986) Isotopic variations of the fixed nitrogen in metamorphic rocks. *Geochimica et Cosmochimica Acta* **50**, 749–58.

Harlaux M, Mercadier J, Marignac C, Villeneuve J, Mouthier B and Cuney M (2019) Origin of the atypical Puy-les-Vignes W breccia pipe (Massif Central, France) constrained by trace element and boron isotopic composition of tourmaline. *Ore Geology Review* **114**, 103132. doi: 10.1016/j.oregeorev.2019.103132.

Hedenquist JW and Lowenstern JB (1994) The role of magmas in the formation of hydrothermal ore deposits. *Nature* **370**, 519–27.

Hoffman EL (1992) Instrumental neutron activation in geoanalysis. *Journal of Geochemical Exploration* **44**, 297–319.

Hollister VF (1978) *Geology of the Porphyry Copper Deposits of the Western Hemisphere*. New York: Society of Mining Engineers of the American Institute of Mining, Metallurgical and Petroleum Engineers, 219 pp.

Inoue A, Utada M and Wakita K (1992) Smectite-to-illite conversion in natural hydrothermal systems. *Applied Clay Science* **7**, 131–45.

Italiano F, Kis MB, Baciu C, Ionescu A, Harangi S and Palcsu L (2017) Geochemistry of dissolved gases from the Eastern Carpathians – Transylvanian Basin boundary. *Chemical Geology* **469**, 117–28.

Iyer K, Schmid DW, Planke S and Millett J (2017) Modelling hydrothermal venting in volcanic sedimentary basins: impact on hydrocarbon maturation and paleoclimate. *Earth and Planetary Science Letters* **467**, 30–42.

Jackson ML (1975) *Soil Chemical Analysis: Advanced Course*. Madison, Wisconsin: M. L. Jackson, 895 pp.

Jamtveit B, Svensen H, Podladchikov Y and Planke S (2004) Hydrothermal vent complexes associated with sill intrusions in sedimentary basins. In *Physical Geology of High-Level Magmatic Systems* (eds C Breitkreuz and N Petford), pp. 233–41. Geological Society of London, Special Publication no. 234.

Jebrak M (1997) Hydrothermal breccias in vein-type ore deposits: a review of mechanisms, morphology and size distribution. *Ore Geology Review* **12**, 111–34.

Klusman RW, Leopold ME and LeRoy MP (2000) Seasonal variation in methane fluxes from sedimentary basins to the atmosphere: results from chamber measurements and modeling of transport from deep sources. *Journal of Geophysical Research* **105**, 661–70.

Krézsek C and Bally AW (2006) The Transylvanian Basin (Romania) and its relation to the Carpathian fold and thrust belt: insights in gravitational salt tectonics. *Marine and Petroleum Geology* **23**, 405–42.

Krézsek C, Filipescu S, Silye L, Maţenco L and Doust H (2010) Miocene facies associations and sedimentary evolution of the Southern Transylvanian Basin (Romania): implications for hydrocarbon exploration. *Marine and Petroleum Geology* **1170**, 191–214.

Krooss BM, Littke R, Muller B, Frielingsdorf J, Schwochau K and Idiz EF (1995) Generation of nitrogen and methane from sedimentary organic matter: implications on the dynamics of natural gas accumulations. *Chemical Geology* **126**, 291–318.

Laznicka P (1988) *Breccias and Coarse Fragmentites: Petrology, Environments, Associations, Ores*. Developments in Economic Geology vol. 25. Amsterdam: Elsevier, pp. 842.

Lowell JD and Guilbert JM (1970) Lateral and vertical alteration-mineralization zoning in porphyry ore deposits. *Economic Geology* **65**, 373–408.

Mason PRD, Downes H, Thirlwall MF, Seghedi I, Szakács A, Lowry and Mattey D (1996) Crustal assimilation as a major petrogenetic process in the East Carpathian Neogene and Quaternary margin arc, Romania. *Journal of Petrology* **37**, 927–59.

Mason PRD, Seghedi I, Szakács A and Downes H (1998) Magmatic constraints on geodynamic models of subduction in the East Carpathians. *Tectonophysics* **297**, 157–76.

Maţenco L, Krézsek E, Merten S, Schmid S, Cloetingh S and Andriessen P (2010) Characteristics of collisional orogens with low topographic build-up: an example from the Carpathians. *Terra Nova* **22**, 155–65.

https://doi.org/10.1017/S0016756822000851 Published online by Cambridge University Press

McDonough WF and Sun SS (1995) The composition of the earth. *Chemical Geology* **120**, 223–53.

Meyer C and Hemley JJ (1967) Wall rock alteration. In *Geochemistry of Hydrothermal Ore Deposits* (ed. HL Barnes), pp. 166–235. New York: Holt, Rinehart and Winston.

Moore JC and Vrolijk P (1992) Fluids in accretionary prisms. *Reviews of Geophysics* **30**, 113–35.

Münker C, Pfänder JA, Weyer S, Buchl A, Kleine T and Mezger K (2003) Evolution of planetary cores and the Earth–Moon system from Nb/Ta systematics. *Science* **301**, 84–7. doi: 10.1126/science1084662.

Pana D and Erdmer P (1994) Alpine crustal shear-zones and pre-Alpine basement terranes in the Romanian Carpathians and Apuseni Mountains. *Geology* **22**, 807–10.

Paraschiv D (1980) Observatii asupra unor zacaminte de gaze mixte din partea de Est a Depresiunii Transilvaniei. *Studii Cercetari Geologice Geofizice, Seria Geologie* **25**, 83–93.

Pécskay Z, Edelstein O, Seghedi I, Szakács A, Kovacs M, Crihan M and Bernad A (1995) K-Ar datings of Neogene–Quaternary calc-alkaline volcanic rocks in Romania. *Acta Volcanology* **7**, 53–61.

Peltz S, Peltz M and Botar N (1982a) Observations litogeochimiques et implications metallogeniques dans l'aire volcanique de Gaineasa (Seaca – Tatarca, Monts Gurghiu). *Comptes Rendus de Institute de Géologie et Géofisique, Bucharest* **LXVII/2**, 81–110.

Peltz S, Tanasescu A and Vâjdea E (1982b) Distributia U, Th, K in structura eruptiva complexa Zebrac-Mermezeu Muntii Calimani de Sud. *Comptes Rendus de Institute de Géologie et Géofisique, Bucharest* **LXVII/1**, 215–37.

Peltz S, Vâjdea E, Balogh K and Pécskay Z (1987) Contributions to the chronological study of the volcanic processes in the Călimani and Harghita Mountains (East Carpathians, Romania). *Comptes Rendus de Institute de Géologie et Géofisique, Bucharest* **72–73/1**, 323–38.

Perry VA (1961) The significance of mineralized breccia pipes. *Mining Engineering* **13**, 367–76.

Petit S, Righi D and Madejová J (2006) Infrared spectroscopy of NH_4^+-bearing and saturated clay minerals: a review of the study of layer charge. *Applied Clay Science* **34**, 22–30.

Procesi M, Ciotoli G, Mazzini A and Etiope G (2019) Sediment-hosted geothermal systems: review and first global mapping. *Earth-Science Reviews* **192**, 529–44. doi: 10.1016/j.earscirev.2019.03.020.

Rădulescu D, Peter E, Stanciu C, Stefanescu M and Veliciu S (1981) Asupra anomaliilor geotermice din sudul muntilor Harghita. *Studii Cercetari Geologice Geofizice* **26**, 169–84.

Reimold WU (1998) Exogenic and endogenic breccias: a discussion of major problematics. *Earth-Science Reviews* **43**, 25–47.

Rohrman M (2007) Prospectivity of volcanic basins: trap delineation and acreage derisking. *American Association of Petroleum Geologists Bulletin* **91**, 915–39.

Roure F, Roca E and Sassi W (1993) The Neogene evolution of the outer of a foreland/fold-and-thrust belt system. *Sedimentary Geology* **86**, 177–201.

Royden LH (1988) Late Cenozoic tectonics of the Pannonian Basin System. In *The Pannonian Basin: A Study in Basin Evolution* (eds LH Royden and F Horváth), pp. 27–48. American Association of Petroleum Geologists Memoir no. 45.

Rubin JN, Henry CD and Price JG (1993) The mobility of zirconium and other "immobile" elements during hydrothermal alteration. *Chemical Geology* **110**, 29–47.

Rudnick RL and Gao S (2003) Composition of the continental crust. In *Treatise on Geochemistry, Volume 3* (eds HD Holland and KK Turekian), pp. 1–64. Oxford: Elsevier.

Sakata S, Sano Y, Maekawa T and Igari SI (1997) Hydrogen and carbon isotopic composition of methane as evidence for biogenic origin of natural gases from the green tuff basin, Japan. *Organic Geochemistry* **26**, 399–407. doi: 10.1016/S0146-6380(97)00005-3.

Sano Y and Williams SN (1996) Fluxes of mantle and subducted carbon along convergent plate boundaries. *Geophysical Research Letters* **23**, 2749–52.

Scholz CH (1990) *The Mechanics of Earthquakes and Faulting*. Cambridge: Cambridge University Press, 439 pp.

Schutter SR (2003a) Hydrocarbon occurrence and exploration in and around igneous rocks. In *Hydrocarbons in Crystalline Rocks* (eds N Petford and KJW McCaffrey), pp. 7–33. Geological Society of London, Special Publication no. 214. doi: 10.1144/GSL.SP.2003.214.01.03.

Schutter RS (2003b) Occurrences of hydrocarbons in and around igneous rocks. In *Hydrocarbons in Crystalline Rocks* (eds N Petford and KJW McCaffrey), pp. 35–68. Geological Society of London, Special Publication no. 214. doi: 10.1144/GSL.SP.2003.214.01.03.

Seghedi I, Balintoni I and Szakács A (1998) Interplay of tectonics and Neogene post-collisional magmatism in the intracarpathian area. *Lithos* **45**, 483–99.

Seghedi I and Downes H (2011) Geochemistry and tectonic development of Cenozoic magmatism in the Carpathian–Pannonian region. *Gondwana Research* **20**, 655–72.

Seghedi I, Downes H, Szakács A, Mason PRD, Thirlwall MF, Rosu E, Pécskay Z, Márton E and Panaiotu C (2004) Neogene–Quaternary magmatism and geodynamics in the Carpathian–Pannonian region: a synthesis. *Lithos* **72**, 117–46.

Shannon RD (1976) Revised effective ionic radii and systematic studies of interatomic distances in halides and chalcogenides. *Acta Crystallographica* **A32**, 751–67.

Sibson RH (1977) Fault rocks and fault mechanisms. *Journal of the Geological Society, London* **133**, 191–213.

Sibson RH (1986) Brecciation processes in fault zones: inferences from earthquake rupturing. *Pure Applied Geophysics* **124**, 159–75.

Sillitoe R (1985) Ore-related breccias in volcano plutonic arcs. *Economic Geology* **80**, 1467–514. doi: 10.2113/gsecongeo.80.6.1467.

Sillitoe R (2010) Porphyry copper systems. *Economic Geology* **105**, 3–41.

Sillitoe RH, Halls C and Grant JN (1975) Porphyry tin deposits in Bolivia. *Economic Geology* **70**, 913–27.

Sillitoe RH and Sawkins FJ (1971) Geologic, mineralogic and fluid inclusions studies relating to the origin of copper-bearing tourmaline breccia pipes, Chile. *Economic Geology* **66**, 1028–41.

Sinclair WD (2007) Porphyry deposits. In *Mineral Deposits of Canada: A Synthesis of Major Deposit-Types, District Metallogeny, the Evolution of Geological Provinces, and Exploration Methods* (ed. WD Goodfellow), pp. 223–43. Geological Association of Canada, Mineral Deposits Division, Special Publication no. 5.

Sruoga P and Rubinstein N (2007) Processes controlling porosity and permeability in volcanic reservoirs from the Austral and Neuquen basins, Argentina. *American Association of Petroleum Geologists Bulletin* **91**, 115–29.

Stanciu C (1976) Transformari hidrotermale in craterul Ostoros. *Comptes Rendus de Institute de Géologie et Géofisique, Bucharest* **LXII**, 199–213.

Stanciu C (1984) Hypogene alteration of Neogene volcanism of the East Carpathians. *Annuaire de L'Institute de Géologie et de Géophysique, Bucharest* **LXIV**, 182–93.

Stanciu C, Udrescu C and Medesan A (1984) The geochemical characterization of the Madarasul Mare hypogene alteration. *Comptes Rendus de Institute de Géologie et Géofisique, Bucharest* **LXVIII**, 341–70.

Svensen H, Bebout G, Kronz A, Li L, Planke S, Chevallier L and Jamtveit B (2008) Nitrogen geochemistry as a tracer of fluid flow in a hydrothermal vent complex in the Karoo Basin, South Africa. *Geochimica et Cosmochimica Acta* **72**, 4929–47.

Svensen H, Jamtveit B, Planke S and Chevallier L (2006) Structure and evolution of hydrothermal vent complexes in the Karoo Basin, South Africa. *Journal of the Geological Society, London* **163**, 671–82.

Svensen H, Planke S, Chevallier L, Malthe-Sorenssen A, Corfu F and Jamtveit B (2007) Hydrothermal venting of greenhouse gases triggering Early Jurassic global warming. *Earth and Planetary Science Letters* **256**, 554–66.

Svensen H, Planke S, Jamtveit B and Pedersen T (2003) Seep carbonate formation controlled by hydrothermal vent complexes: a case study from the Voring Basin, the Norwegian Sea. *Geo-Marine Letter* **23**, 351–8.

Szakács A and Krézsek C (2006) Volcano–basement interaction in the Eastern Carpathians: explaining unusual tectonic features in the Eastern Transylvanian Basin, Romania. *Journal of Volcanology and Geothermal Research* **158**, 6–20.

Szakács A and Seghedi I (1995) The Călimani-Gurghiu-Harghita volcanic chain, Eastern Carpathians, Romania: volcanological features. *Acta Vulcanology* **7**, 145–53.

Taylor RG and Pollard PJ (1993) *Mineralized Breccia Systems: Methods of Recognition and Interpretation*. Contributions to the Economic Geology Research Unit no. 46. Townsville: Key Center in Economic Geology, James Cook University of North Queensland, 31 pp.

Tiliță M, Maţenco L, Dinu C, Ionescu L and Cloetingh S (2013) Understanding the kinematic evolution and genesis of a back-arc continental "sag" basin: the Neogene evolution of the Transylvanian Basin. *Tectonophysics* **602**, 237–58.

Tiliță M, Scheck-Wenderoth M, Maţenco L and Cloetingh S (2015) Modelling the coupling between salt kinematics and subsidence evolution: inferences for the Miocene evolution of the Transylvanian Basin. *Tectonophysics* **658**, 169–85.

Tomarua H, Lu Z, Fehn U and Muramatsu Y (2009) Origin of hydrocarbons in the Green Tuff region of Japan: ^{129}I results from oil field brines and hot springs in the Akita and Niigata Basins. *Chemical Geology* **264**, 221–31. doi: 10.1016/j.chemgeo.2009.03.008.

Vaselli O, Minissale A, Tassi F, Magro G, Seghedi I, Ioane D and Szakács A (2002) A geochemical traverse across the Eastern Carpathians Romania: constraints on the origin and evolution of the mineral water and gas discharges. *Chemical Geology* **182**, 637–54.

Wang PJ, Feng ZQ, Liu WZ and Chen SM (2008) *Volcanic Rocks in Petroliferous Basins: Petrography, Facies, Reservoir, Pool, Exploration*, pp. 99–161. Beijing: Sciences Press (in Chinese with English abstract).

Whiticar MJ (1999) Carbon and hydrogen isotope systematics of bacterial formation and oxidation of methane. *Chemical Geology* **161**, 291–314.

Williams LB and Hervig RL (2006) Crystal size dependence of illite-smectite isotope equilibration with changing fluids. *Clays and Clay Minerals* **54**, 531–40.

Wright AE and Bowes DR (1963) Classification of volcanic breccias: a discussion. *Geological Society of America Bulletin* **74**, 79–86.

Wright JV, Smith AL and Self S (1980) A working terminology of pyroclastic deposits. *Journal of Volcanology and Geothermal Research* **8**, 315–36.

Zhang J, Amakawa H and Nozaki Y (1994) The comparative behaviors of yttrium and lanthanides in the seawater of the North Pacific. *Geophysical Research Letters* **21**, 2677–80.

Zhang L, Yang L-Q, Weinberg RF, Groves DI, Wang Z-L, Li G-W, Liu Y, Zhang C and Wang Z-K (2019) Anatomy of a world-class epizonal orogenic-gold system: a holistic thermochronological analysis of the Xincheng gold deposit, Jiaodong Peninsula, eastern China. *Gondwana Research* **70**, 50–70.

Zhu Y, Shi B and Fang C (2000) The isotopic compositions of molecular nitrogen: implications on their origins in natural gas accumulations. *Chemical Geology* **164**, 321–30.

https://doi.org/10.1017/S0016756822000851 Published online by Cambridge University Press